Marine vibrators: the new phase of seismic exploration

R.M. Laws[1], D. Halliday[1*], J.-F. Hopperstad[1], D. Gerez[2], M. Supawala[2], A. Özbek[1], T. Murray[2] and E. Kragh[1]

[1]*Schlumberger Cambridge Research, High Cross, Madingley Road, Cambridge, CB3 0EL, United Kingdom of Great Britain and Northern Ireland, and* [2]*WesternGeco, Oslo, Norway*

ABSTRACT

Marine seismic vibrators are generally considered to be less intrusive than airguns from an environmental perspective. This is because they emit their energy spread out in time, rather than in a single, high-intensity pulse. There are also significant geophysical benefits associated with marine vibrators, and they stem from the ability to specify in detail the output acoustic waveform. The phase can be specified independently at each frequency. Such detailed control cannot be achieved with conventional airgun sources, where the phase can only be modified using simple overall time delays. The vibrator phase can be employed in several different ways: it can be applied to the overall source phase in a sequence so that it varies from one source point to the next; it can be applied to the individual vibrators within the source array so the source directivity is changed; it can be applied to the overall source phase of each source in a simultaneous source acquisition. Carefully designed phase sequences can attenuate the residual source noise, and this in turn allows extra source points to be interleaved between the conventional ones. For these extra source points, the relative phase of the vibrators within the array can be chosen to create a transverse gradient source, which illuminates the earth predominantly in directions out of the plane of the sail line without left/right ambiguity. If seismic vibrator data are acquired using interleaved conventional and transverse gradient sweeps, more information is collected per kilometre of vessel travel than is the case in conventional acquisition. This richer data acquisition leads to the possibility of acquiring all the necessary seismic data in a shorter time. Three-dimensional reconstruction techniques are used to recover the same image quality that would have been obtained using the conventional, more time-consuming acquisition. For a marine vibrator to be suitable for these techniques it must, in general terms, have 'high fidelity'. The precise device specifications are defined through realistic end-to-end simulations of the physical systems and the processing. The specifications are somewhat more onerous than for a conventional vibrator, but they are achievable. A prototype vibrator that satisfies these requirements has been built. In a simulated case study of a three-dimensional deep-water ocean bottom node survey, the seismic data could have been acquired using marine vibrators in one third of the time that it would have taken using airguns.

Key words: Acquisition, Imaging, Seismics.

---

*E-mail: dhalliday@slb.com
All authors are with Schlumberger.

1 INTRODUCTION

The environmental advantage of marine vibrators over airguns has historically been the main driver for their development. Perhaps the first example of this was a survey in the Caspian Sea in the early 1980s. It was said that marine vibrators were used instead of airguns because the caviar was more valuable than the oil. Other early uses of marine seismic vibrators were described by Bird, Peacock and Walker (1984), Haldorsen, Desler and Chu (1985) and Johnson, Thompson and Walker (1988). They also found favour in transition zone applications (Potter *et al.* 1997). In more recent times, concern about the possible impact of airgun signals on marine life has led to a revival of interest in the marine vibrator. For example, an industry consortium to develop a viable marine vibrator has been established (see Feltham *et al.* 2017, who give a more detailed history and further references).

In this paper, however, we concentrate on the geophysical advantages of the marine vibrator rather than the environmental advantages. One geophysical advantage of marine vibrators over airguns is that the *phase* of the vibrator output waveform is controllable, whereas the phase of an airgun pulse can only be modified by a simple time delay. Exploiting the ability to control phase can significantly improve the efficiency of marine seismic data acquisition.

A perceived geophysical disadvantage of marine vibrators with respect to airguns has been widely discussed in the past: vibrator arrays were found to lack low-frequency energy compared with airguns. However, several studies have shown that airgun arrays often produce more energy in some parts of the spectrum than is actually needed (see, for example, Laws, Kragh and Morgan 2008). This means that attempting to make the vibrator spectrum match that of an airgun array at all frequencies might not be necessary. In this paper, it is shown how the spectrum of the vibrator source can be optimally specified and delivered; the spectrum requirement is based on the required image signal-to-noise ratio (SNR) rather than on the requirement to 'do what the airgun does'.

There are several differences between marine and land vibrators. In the marine case, the 'move-up' time between source points is very short; the vessel moves at an almost constant speed and ideally each sweep would begin immediately after the previous one had finished. Use of such 'cascaded sweeps' puts extra requirements on the harmonics of the emitted waveform. Cascaded sweeps are discussed by Moerig, Barr and Nyland (2002). In the land case, the deconvolved harmonics can be placed off the end of the seismic record and muted out, but in the cascaded sweep marine case the whole of the record

is used in the production of the image. Fortunately, a second difference between the marine and land situations helps to solve this problem: in the marine case the distortion can be kept low and the emitted waveform can be measured very accurately because the surrounding water has well-defined, linear properties.

A geophysical disadvantage of airgun sources is that a large temporal source interval is needed so that the residual source noise (RSN) can decay to an acceptably low level. Landrø (2008) discusses this issue in detail. Typically, a 10-second interval is left between airgun source activations, and this results in a spatial source interval that is larger than would be ideal on spatial sampling grounds. In this paper, it is shown how the marine vibrator allows this limitation to be removed and how the resulting extra source points can be best used.

One of the geophysical advantages of marine vibrators over airguns is that of efficiency. The seismic data can be acquired in a much shorter time if the phase control of the vibrator is fully exploited. In this paper we discuss, as an example, a three-dimensional (3D) deep-water ocean bottom node (OBN) survey. We show that the survey could have been acquired in one third of the time using marine vibrators compared to the time it would have taken using airguns.

1.1 Using the phase of the vibrator waveform

There are three distinct uses of phase in a survey using marine vibrators. The first use is the variation of phase from one source point to the next (phase sequencing); the second is the variation of phase within the elements of the source array; the third the variation of the phase between the sources in a simultaneous source acquisition. These uses are all valuable and can be combined. Next we discuss the first two uses further.

The first use of vibrator phase is to attenuate RSN using phase sequencing. Phase sequencing allows us to manipulate the frequency-wavenumber (*f-k*) spectrum in common receiver domain (CRD) and to move the RSN away from the signal. This makes it easy to remove. We use the attenuation of RSN to insert extra sweeps between the 'conventional' sweeps so that we can collect more information during the same source line.

An alternative use of a shorter source-time repetition interval is to sail the source vessel faster, and thus retain a conventional spatial source repetition interval. This approach is not discussed further herein, but it would lead to faster acquisition if the operational difficulties of fast towing could be overcome.

The second use of the vibrator phase is to modify the directivity of the array. We can do this by changing the relative phases of the individual vibrator units relative to each other. If, for example we distribute the vibrators in laterally separated pairs, we can modify the lateral directivity of the source. We can make the directivity change from one sweep to the next if we wish.

The combined use of phase sequencing for RSN removal and alternating source directivity enables us to collect two complementary sets of information at the same time during a single source line. For example, we might collect a conventional source line with a conventional source point separation and, at the same time, use the extra interleaved source points to acquire a special line with a transverse horizontal gradient source. We collect more information during the line than we could collect using a conventional acquisition.

The information about both earth's monopole response and its transverse gradient response can be combined using reconstruction techniques. Because more information is acquired during each line it turns out that we do not need to acquire so many lines; we can generate the same image quality using fewer source lines.

In the first section of the paper, we show in detail how phase sequencing enables us to insert extra sweeps into the source line and to separate simultaneous sources of high multiplicity. Phase sequencing cannot be used with an airgun source because there is no control of phase other than simple time delays. The methods are closely related to those given by Laws (2012a), Laws and Halliday (2013) and have also been discussed by Laws *et al.* (2016) and Halliday *et al.* (2017). In addition, phase sequencing can be used to aid the separation of simultaneous sources leading to much higher multiplicities than can be used with conventional methods (Laws *et al.* 2016, and see Moore *et al.* 2008 for a general discussion). These phase-sequencing techniques are primarily of value for marine seismic vibrators. Related techniques have been proposed for use with airguns (Robertsson, Amundsen and Pedersen 2016), but the phase control in airguns is confined to what can be created by applying time shifts, and that is very limiting (Halliday and Moore 2018).

In the second section, we look at the design of sweeps and the source array configuration. First, we explain how the use of non-linear vibrator frequency sweeps and multiple depths are used to create the desired spectrum. We also explain how the desired spectrum is based on the image SNR, rather than on a requirement to match the conventional airgun spectrum. We also mention another aspect of sweep design: the use of rapid transitions from one frequency to another.

In the third section, we show how to use the extra inserted sweeps to measure the earth's response to a transverse gradient source (an approximation to a horizontal crossline dipole). This is what enables us to collect much more information from a single seismic line and enables us to create the same image using fewer lines. We simulate the seismic experiment using a realistic 3D finite difference calculation. For this section, the simulated dataset is for a realistic earth, but there is no noise present, no perturbations, no errors and the sea is flat. We show that the image agrees excellently with the conventional image, although it would take only one third of the acquisition time of a corresponding airgun survey.

In the fourth section, we discuss the effect of noise and perturbations to the marine vibrator system. We model, positioning inaccuracies, rough sea effects (on position and on sound scattering), distortion in the emitted wavefield and so on. The effects of all these perturbations can be studied by simulation and their effect on the image determined. Such studies lead directly to the specifications for the vibrators themselves, the method for measuring their positions and output waveforms, the acceptable levels of distortion and for the towing and handling system that is needed to maintain the vibrators in the correct place in the water.

In the fifth section, we illustrate the current design of a physical vibrator that satisfies the requirements we have identified. An early, scaled-down prototype was built and tested in 2012 and the finished design, together with the deployment method, integrated closed-loop control and associated systems, is almost ready for production. The system is designed to satisfy the DNV GL standard for underwater technology, ensuring reliability and safety. Power is supplied via an electrical umbilical which also includes the fibre optic data links.

In the sixth section, we briefly summarize why marine vibrators are potentially less intrusive for marine mammals, fish and sea turtles than airguns are. We finish the paper with conclusions on the use of marine vibrators for efficient marine surveying.

2 PHASE SEQUENCING

In this section, we discuss how the control of the phase of the marine vibrator source waveform can be used to reduce residual source noise (RSN) thereby potentially enabling more information to be collected per kilometre of survey line. In seismic surveying, the source repetition time interval is often longer than would be geophysically ideal; this is done, *inter alia*, to allow the RSN to decay to an acceptable level. Phase

sequencing allows us to remove the RSN and thus reduce the source-time interval.

We have simulated the impact of RSN in a marine survey using real (airgun) seismic data that were acquired with a source-time interval of 12 seconds. The data have been overlapped and added in the computer to simulate a common receiver gather acquired with a source-time interval of 5 seconds. This creates a quasi-realistic dataset in which we know exactly what is signal and what is RSN. This dataset does not include acquisition artefacts specific to a marine vibrator (such as a moving source), but it is still suitable to demonstrate the impact of RSN (we consider these more realistic acquisition effects in Sections 3 and 4). An example is shown in Fig. 1. The area in the *f-k* spectrum marked with the red triangle was termed 'the empty quarter' by Laws and Halliday (2013); there is no signal in it. The empty quarter is bounded by the water velocity and the spatial Nyquist number. The top right panel shows the effect on the RSN of zeroing the empty quarter; in this case there is no effect because there is no signal or noise there anyway. The top right panel of Fig. 1 will be compared in due course to the corresponding panels of Figs. 2 and 3 where phase sequencing is used, that is to say, when the source phase is changed from one source point to the next.

2.1 Simple 'sine and cosine' phase sequencing

A basic phase sequence is to apply a 90° phase shift to alternate sweeps (the same phase shift at all frequencies). This is the same as making the vibrator alternate between the sine and cosine of the sweep. There is no effect on the emitted energy spectrum or on the source directivity. The phase shift is applied to all the vibrators in the source array. Once the basic (0° shifted) sweep has been deconvolved, only the [0°, 90°, 0°, 90°, 0° and so on] sequence remains. We can simulate this simply by applying a 90° phase shift to alternate shots of the airgun data discussed above.

The remaining [0°, 90°, 0°, 90°, 0° and so on] phase shift in the recorded data will next be removed through deconvolution using each emitted sweep. However, the RSN, which originated from the preceding source, will thereby be deconvolved with a different phase from the one that it was emitted with.

Table 1 shows how this simple phase sequence propagates through source deconvolution. The top row of Table 1 shows the sweep number (for some arbitrary part of the line). The second row shows the phase of the emitted signal. The third row shows the phase of the emitted RSN; this is the same as the phase of the preceding sweep. The fourth row shows the phase of the source deconvolution operator that

undoes the phase shift of the emitted signal. The deconvolved signal then has a constant zero phase as shown in the fifth row. The signal will look quite normal; the alternating sequence of source phases has been removed by the deconvolution. But, as if by magic, the RSN (shown in the bottom row) ends up with a phase that flips polarity from one trace to the next. This is a very powerful result, and it makes the RSN very easy to remove.

Figure 2 shows the effect of this simple phase sequencing. The RSN (upper middle) reverses sign trace by trace and, as a result, it does not look at all like a seismic wavefield. In the *f-k* domain it is shifted along the wavenumber axis by a distance equal to the Nyquist wavenumber. This places the RSN halfway between the repeating signal spectra – directly into the empty quarter. The signal is left in its original position, so the empty quarter can be zeroed with no effect on the signal. The RSN is greatly attenuated using phase sequencing (upper right of Fig. 2 compared to upper right of Fig. 1). A small part of the RSN (including the RSN of the sweep before the previous one which is still located near $k = 0$) lies outside the empty quarter and is not removed.

2.2 More elaborate phase sequences

In the previous section we discussed a source phase that alternated between 0° and 90° sweep by sweep, giving an RSN phase increment of 180°/trace in the common receiver domain (CRD). In fact this is a special case of a more general situation where the RSN has some chosen phase increment per trace. An advantage of more elaborate phase sequences can be seen if we consider the RSN of the sweep before the previous sweep. By choosing 120°/trace increment, we are able to fit more of the RSN of the two preceding sources into the 'empty quarter'. To do this, we need to use a more elaborate phase sequence. Instead of repeating the two value sequence [0°, 90°] we need to use the repeating six value sequence [0°, 60°, 0°, 180°, −120°, 180°].

Laws and Halliday (2013) showed this relationship (equation (1)), between the desired RSN phase increment θ and the required phase sequence, $\varphi(n)$ that would create it.

$$\varphi(n) = 2\varphi(n-1) - \varphi(n-2) - \theta. \tag{1}$$

For a 120° increment per trace for the RSN in the CRD equation (1) generates the [0°, 60°, 0°, 180°, −120°, 180°] as used above. This scheme is illustrated in Table 2 and the results are shown in Fig. 3. In the middle panels of Fig. 3 the RSN from the previous source activation, and from the sweep before that, are both moved into the empty quarter. The upper
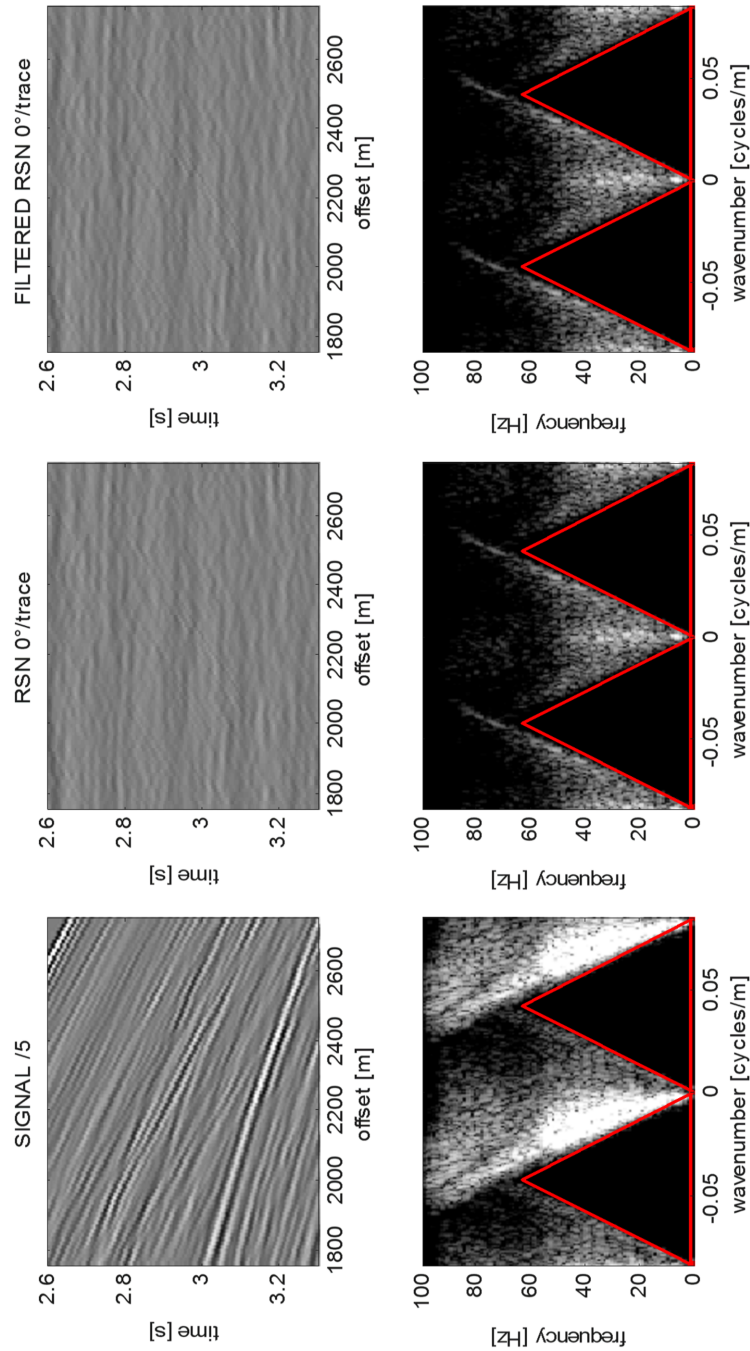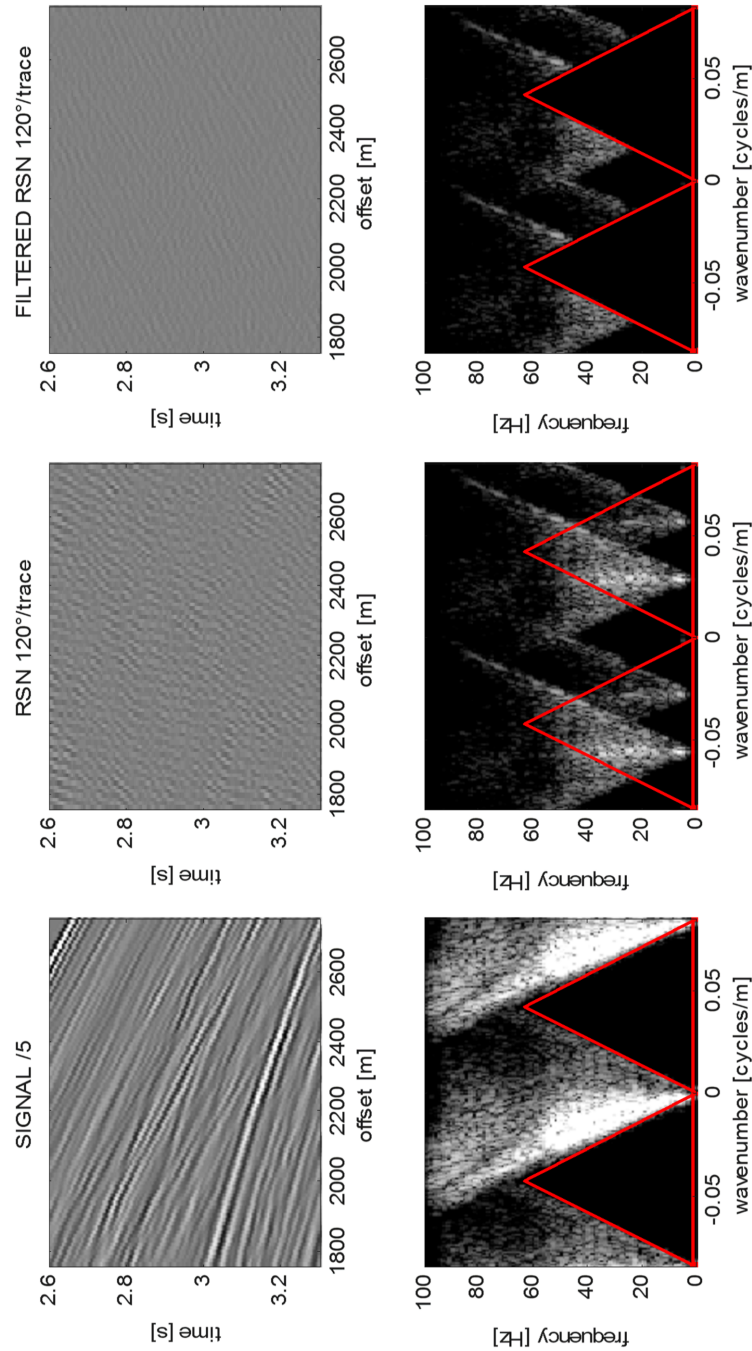
Figure 1 An example window from a semi-synthetic dataset in the common receiver domain (CRD; see text) using no phase sequencing; SIGNAL (scaled down by a factor of 5); RSN; filtered RSN. Lower row: the *f*-*k* spectra of the upper row.
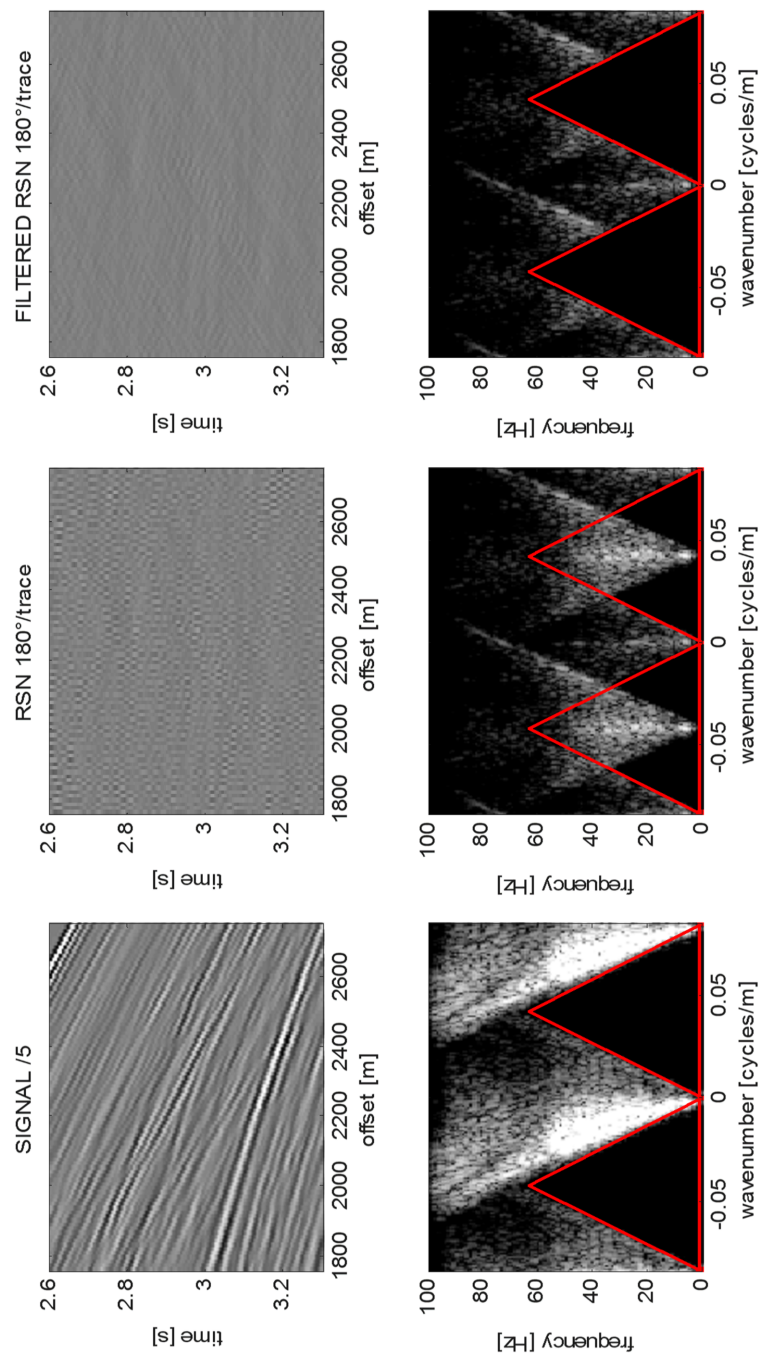
Figure 2 An example window from a semi-synthetic dataset in the common receiver domain (CRD) using a [0°, 90°, 0°, 90°, 0° and so on] phase sequence. To see the power of the method, compare the top right panel in this figure with the top right panel of Fig. 1.

Figure 3 An example window from a semi-synthetic dataset in the common receiver domain (CRD) using a [0°, 60°, 0°, 180°, −120°, 180°] phase sequence. To see the power of the method, compare the top right panel in this figure with the top right panel of Fig. 1.

Table 1 A simple phase sequence

Sweep number	91	92	93	94	95	96	97
Source phase, $\varphi(n)$ (alternating *sine* and *cosine*)	0°	90°	0°	90°	0°	90°	0°
RSN phase (same as preceding sweep)	90°	0°	90°	0°	90°	0°	90°
Deconvolution operator phase (reverse of signal phase)	0°	−90°	0°	−90°	0°	−90°	0°
Deconvolved source phase (zero by design)	0°	0°	0°	0°	0°	0°	0°
Deconvolved RSN phase (incrementing 180° per sweep)	90°	−90°	90°	−90°	90°	−90°	90°

The sweeps alternate between 0° and 90°. After source deconvolution it is found that the RSN reverses polarity from one sweep to the next, but the signal does not. This is a very powerful result.

Table 2 A more elaborate phase sequence

| Sweep number	91	92	93	94	95	96	97
Source phase, $\varphi(n)$ (special six-fold sequence)	0°	60°	0°	180°	−120°	180°	0°
RSN phase (same as preceding sweep)	180°	0°	60°	0°	180°	−120°	180°
Deconvolution operator phase (reverse of signal phase)	0°	−60°	0°	−180°	120°	−180°	0°
Deconvolved source phase (zero by design)	0°	0°	0°	0°	0°	0°	0°
Deconvolved RSN phase (incrementing 120° per sweep)	180°	−60°	60°	180°	−60°	60°	180°

After source deconvolution it is found that the RSN phase advances by 120° from one sweep to the next, but the signal does not.

right panel shows how zeroing the empty quarter attenuates the RSN from *both* preceding sweeps (compare the top right panel of Fig. 3 with that of Fig. 1).

Using phase sequencing to attenuate RSN allows us to emit sweeps more rapidly. This reduction in source-time interval can be used, for example to acquire the survey more quickly by sailing the vessel faster or it could be used (as herein) to 'interleave' extra sweeps with special directivities that are based on a transverse horizontal gradient.

# 3 SWEEP DESIGN AND SOURCE ENERGY

We reprocessed some proprietary test data from 1997 in which similar lines were acquired using both airguns and vibrators. The test area was to the North of Shetland. We confirmed that the vibrator images did indeed lack low-frequency en-
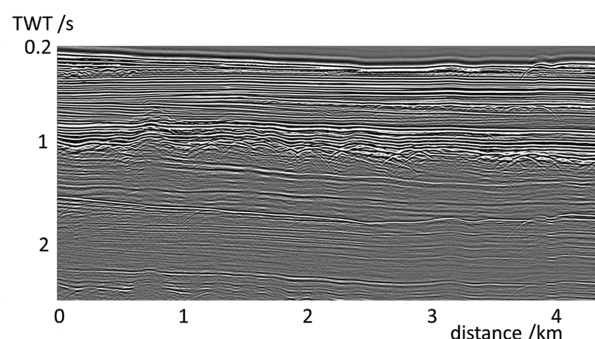
Figure 4 Brute stack of data obtained using an array of six IVI (Industrial Vehicles International, Inc.) marine vibrators.
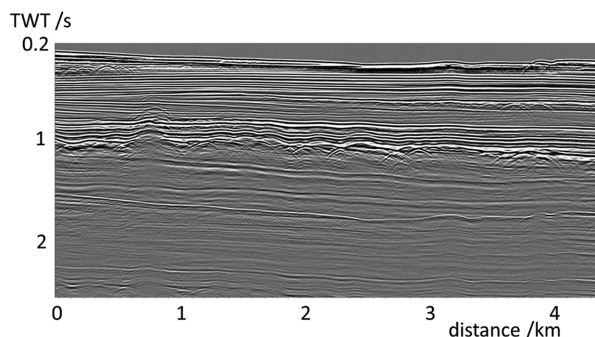
Figure 5 Brute stack of data obtained using an airgun array.

ergy. In the test, six vibrators made by IVI (Industrial Vehicles International, Inc.) were used, with a sweep time of 5 seconds followed by a listening time of 5 seconds. The sweeps were linear over a range 5–83 Hz. The weaker low-frequency content of the vibrator image can be seen by comparing the images in Figs. 4 and 5.

3.1 Increasing the source array output

There are several ways in which the energy spectrum of the vibrator array can be increased, apart from by simply using more vibrators. One way is to arrange that every vibrator in the array emits sound continuously with no separate 'listening time'. This is known as 'cascaded sweeping' in land seismic (Moerig *et al.* 2002). It requires a vibrator whose output has very little harmonic energy because there is no part of the recorded data that are muted out. In the marine case, the acoustic medium (water) is very benign and we are able to emit a low distortion output, and we can also measure exactly what was emitted using the method given by Laws (2013).
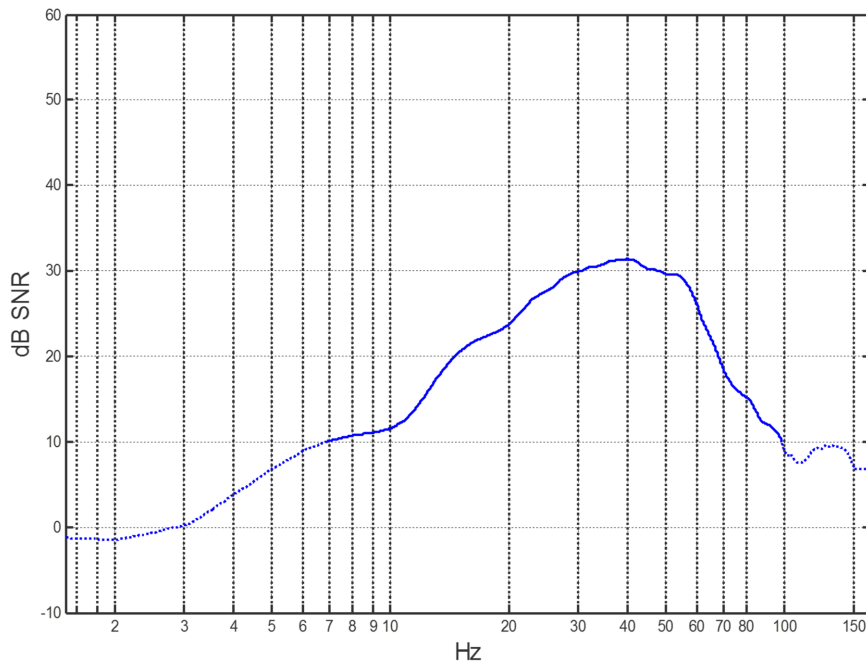
Another way to increase output is to deploy each vibrator at a depth appropriate to its emitted frequency range and ghost response; the low-frequency vibrators would be deep, the high-frequency ones would be shallow (Laws and Morice 1999). This implies, of course, that each vibrator unit emits only a part of the sweep. Such a constraint is also valuable in the design of the units themselves; each one can be optimized for the frequency range it emits.

A further improvement is to emit several frequencies at the same time by the vibrator array. If there are, for example three frequency ranges then they can all be emitted simultaneously.

3.2 Basing the desired source spectrum on the image SNR

The final aspect of optimal source design is to reconsider the required source output spectrum. The goal should be to emit only the energy that is actually required for the image. In the past, it was usual to try to make the marine vibrator array emit a similar energy spectrum to that of the airgun array, but that is not the optimal approach. Typically, in a towed streamer airgun survey, the source emits more high-frequency energy than is needed and rather less low-frequency energy than would be ideal. With the vibrator source we control the frequency sweep function so, using non-linear sweeps, we are able to trade off some high-frequency output in order to increase the low-frequency output.

To define the required source spectrum we need to decide what signal-to-noise ratio (SNR) is required in the image at each frequency at the two-way-time of interest. We then work backwards from the image SNR requirement to the source spectrum energy requirement.

In order to relate the source spectrum to the image SNR, we need experimental or simulated data from a similar area. Several studies (Laws *et al.* 2008; Kragh *et al.* 2012; Halliday *et al.* 2015a) have done this using a 'stealth test'. In such tests, the seismic line is acquired twice. In the first pass a conventional source array is used; in the second pass (the 'stealth' line) the airguns are not fired, but all other noise sources are present. Both conventional and stealth data are processed, in exactly the same way, to produce seismic images, but of course the stealth image contains only noise. By comparing the two images, the SNR can be calculated at each two-way time and at each frequency for the particular source spectrum that was used in the test.

An example of such an SNR curve for a towed streamer survey is shown in Fig. 6. The towed streamer case is more challenging than the ocean bottom node (OBN) case, because the noise is higher. For the towed streamer case shown in Fig. 6, the SNR falls from a peak of 30 dB at 50 Hz to 0 dB at 3 Hz. This is because the dominating flow noise for the streamer increases as the frequency is reduced.

Figure 7 Typical equivalent noise source for towed streamer acquisition. A source with this spectrum would make an image with SNR equal to 1:1 at all frequencies at the chosen TWT.
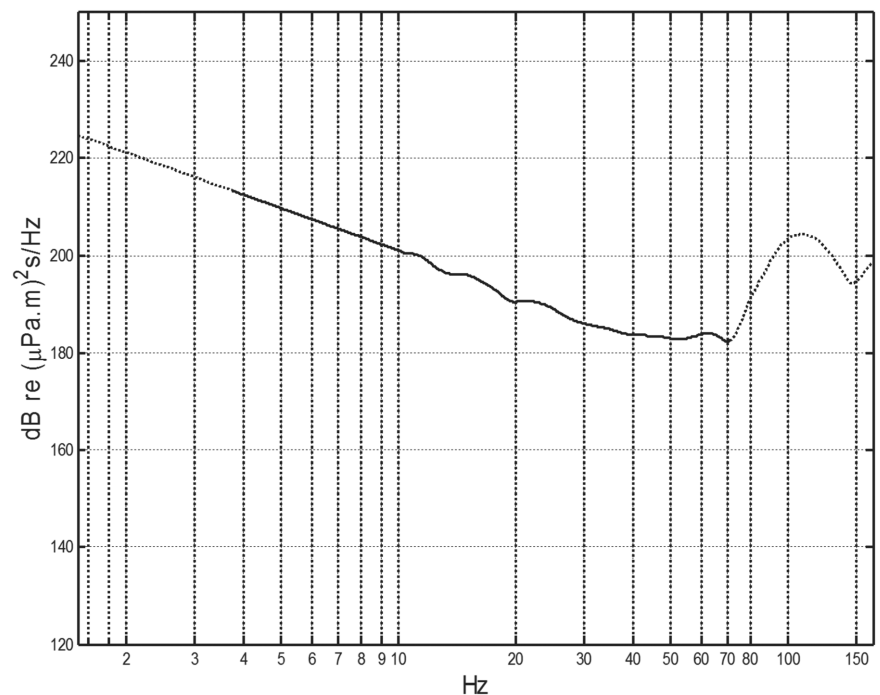
Once the SNR has been determined by a stealth test, it is straightforward to calculate the source spectrum that would have given an SNR of 0 dB at all frequencies in the image. We call this the 'equivalent noise source' and it is shown in Fig. 7.

We then need to decide what SNR is actually required in the image. This is multiplied by (added in decibels) the equivalent noise spectrum to yield the source spectrum requirement, which is in turn used to define the vibrator array.

The design of the sweep is illustrated in Fig. 8. The black curve shows the equivalent noise source spectrum and the grey curve, which is 18 dB higher, is the source spectrum that would give an image SNR of 18 dB. The red curve is the source spectrum of a typical airgun array. The blue curve is the desired vibrator spectrum. In this case we have demanded that the image SNR should be either 18 dB or the SNR that would have been obtained with an airgun array, whichever is lower. The desired vibrator spectrum is limited to the seismic bandwidth.

The vibrator groupings and depths, and the sweeps they emit, are optimized using a global search algorithm. Vibrator groups are favoured for two reasons: first, a group of vibrators emitting the same sweep is more efficient than the same vibrators emitting singly (Laws, Parkes and Hatton 1988); second, groups are needed so that advanced directivity patterns can be emitted. For example, for those frequencies where a trans-
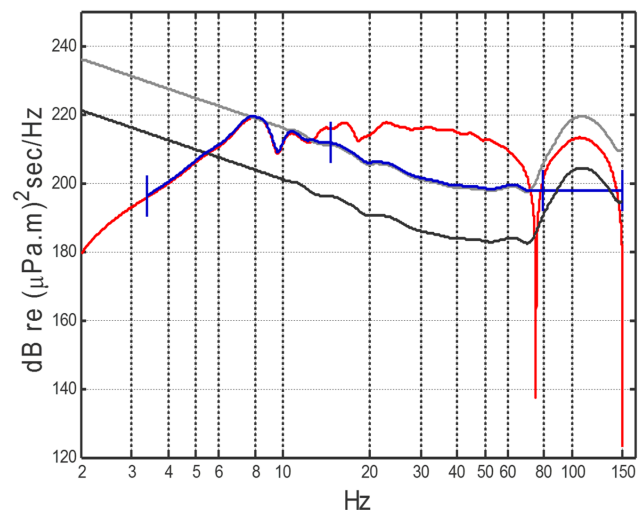
Figure 8 Source spectra. black: equivalent noise source, grey: 18 dB SNR at all frequencies, red: the spectrum of an airgun array, blue: the actual vibrator array spectrum.

verse horizontal gradient is needed, we must have a pair of vibrators spatially separated to the left and right of the sail line. This will be discussed in detail later in this paper. In addition, we have applied an operational constraint such that the vibrators must be at depths between 8 and 30 m and that the frequency sweeps are the same for every source point. We
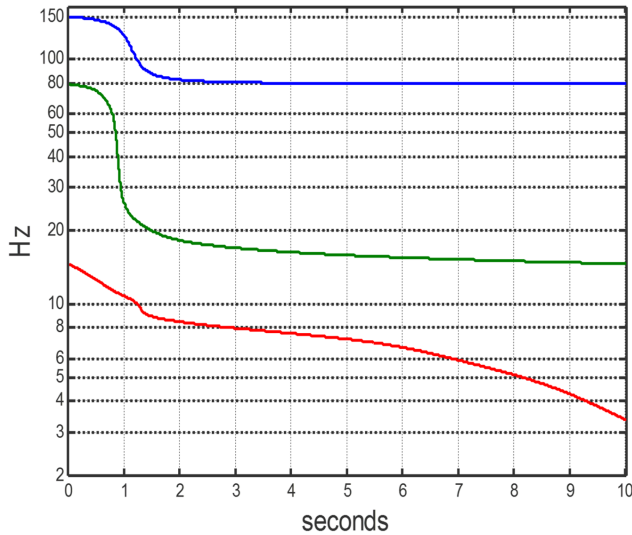
Figure 9 Sweep functions to generate the source spectrum defined to give 18 dB SNR or match the airgun array, whichever is lower. The vibrator array can reach down to 3 Hz. Blue group 1 at 9.5 m, green group 2 at 9 m, red group 3 at 30 m depth.

Figure 10 Sweep functions that generate a source spectrum that matches the airgun array at all frequencies. The vibrator array can only reach down to 10 Hz. Blue group 1 at 9.5 m, green group 2 at 9 m, red group 3 at 30 m depth.
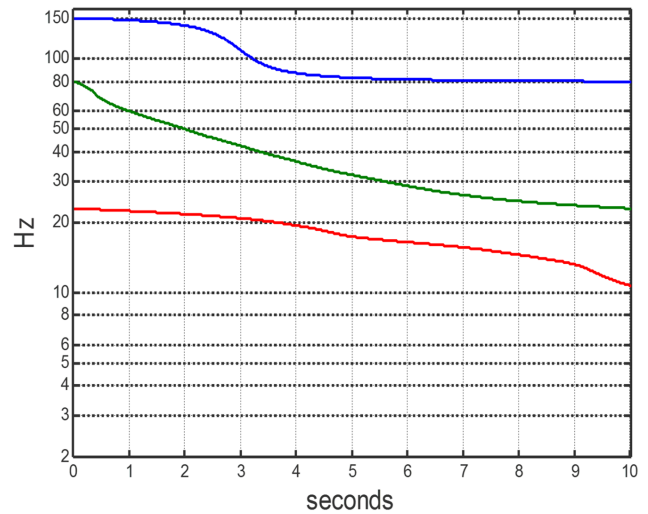
have mandated a top frequency of 150 Hz and a source-time interval (the same for all frequency groups in this case) of 10 seconds. The cost function of the optimization is the lowest emitted frequency. The resulting sweeps are shown in Fig. 9.

Note in Fig. 9 that three frequencies are emitted simultaneously from three groups of vibrators. The highest frequencies are emitted by group 1 that is deployed at 9.5 m and emits between its first and second ghost notch. This choice of depth has resulted from the requirement not to deploy any vibrator shallower than 8 m in this example. Group 2 emits from 80 to 14.6 Hz and is deployed at 9 m. Group 3 emits from 14.6 Hz down to 3.4 Hz and is deployed at 30 m.

Note that the shallow, high-frequency vibrators easily complete most of their emission within 5 seconds, whereas the low-frequency vibrators use the whole available 10 seconds to emit theirs. In principle, the high-frequency vibrators could 'fit in' a repeat sweep (a transverse source gradient, for example).

It is a happy coincidence that the form of the energy-optimal sweeps – a rapid transition through high frequencies and a slow transition through the low frequencies – is broadly what is required for a special class of smear-free sweeps, where the moving source always remains within the changing Fresnel zone of the nominal stationary source position (Laws 2012b).

Figure 10 shows the vibrator spectrum that matches the airgun spectrum. Within the 10-second sweep time, a mini-

mum frequency of 10 Hz is reached, as opposed to the 3.4 Hz reached by the SNR optimized sweep.

Using the SNR optimized sweeps described in this section the lack of low-frequency energy in marine vibrator surveys, which was a significant problem in the 1980s and 1990s, has been overcome.

3.3 Sweep sequence for OBN acquisition including gradient sweeps

The sweeps appropriate to OBN acquisition are different from those designed for towed streamer acquisition because the noise has a different character, for example while low-frequency flow noise is an issue for towed streamer acquisition, it will not be present in the OBN data. In addition, horizontal transverse gradient sweeps are included in the sweep sequence, interleaved between omnidirectional (conventional) sweeps.

To emit an omnidirectional wavefield, two laterally separated vibrators, deployed at the same depth, emit the same signal in phase. To emit a horizontal transverse gradient wavefield, the same two vibrators emit signals with opposite polarity. We alternate the output of the pair of vibrators between an omnidirectional sweep and a gradient sweep. The omnidirectional sweep emits energy with the same polarity in all directions (Fig. 11a), while the gradient sweep emits energy with positive polarity in the positive *y* direction (right),

Figure 11 Crossline radiation patterns in dB as a function of take-off angle for (a) an omnidirectional source and (b) a transverse source gradient. Positive polarities are plotted in red and negative polarities are plotted in blue. The dotted black line indicates the position of the notch on the alternate plot.
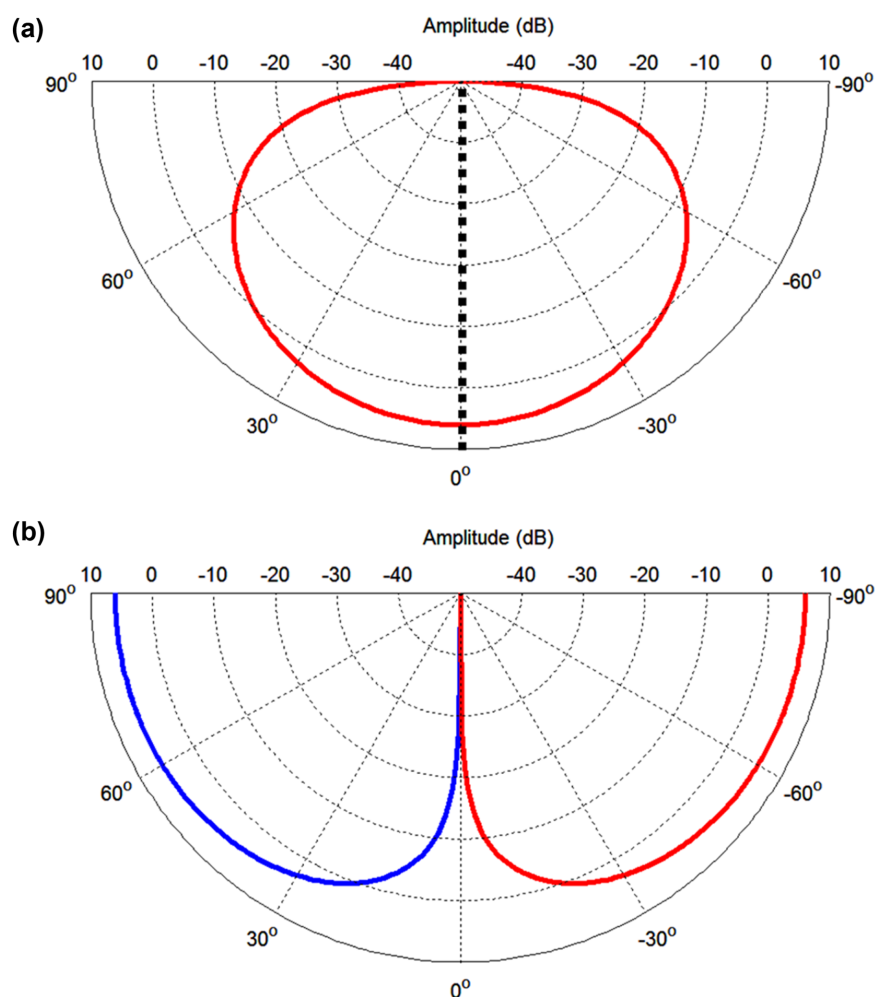
negative polarity in the negative *y* direction (left), and zero energy in the vertical *z* direction (Fig. 11b). Note that the figure appears to show a ghost notch for the omni-directional source, but not for the dipole source. This is not a ghost notch in the conventional sense, but is due to the frequency chosen, which for horizontal take-off angle happens to correspond to destructive interference for the omni-directional source, and constructive interference for the gradient source.

The earth's responses to both omnidirectional sweeps and transverse gradient sweeps contain complimentary information; their nulls do not overlap. In the next section, we show that this allows more accurate reconstruction of the wavefield between source lines and that we can therefore increase the distance between sail lines without reducing the image quality.

Figure 12 shows a typical set of OBN sweeps for the case of acquiring alternating omnidirectional and transverse gradient sweeps. The low-frequency sources emit omnidirectional sweeps with a length of 10 seconds. Due to the longer spatial wavelengths the reconstruction problem is easier to solve at these frequencies, and the extra information from the gradient sweeps is not required. Below 15 Hz, where the gradient is not needed, the whole 10 seconds is used for the sweep and the phase sequence is [0°, 90°, 0°, 90°, 0° and so on] to attenuate the residual source noise (RSN). Above 15 Hz the sweep interval is 5 seconds, but the vibrator pairs are emitting alternating omnidirectional and lateral gradient sweeps. The phases of the vibrators are shown in square brackets in Fig. 12.

The gradient sweeps in this example have slightly different sweeps from the omnidirectional sweeps. This is because
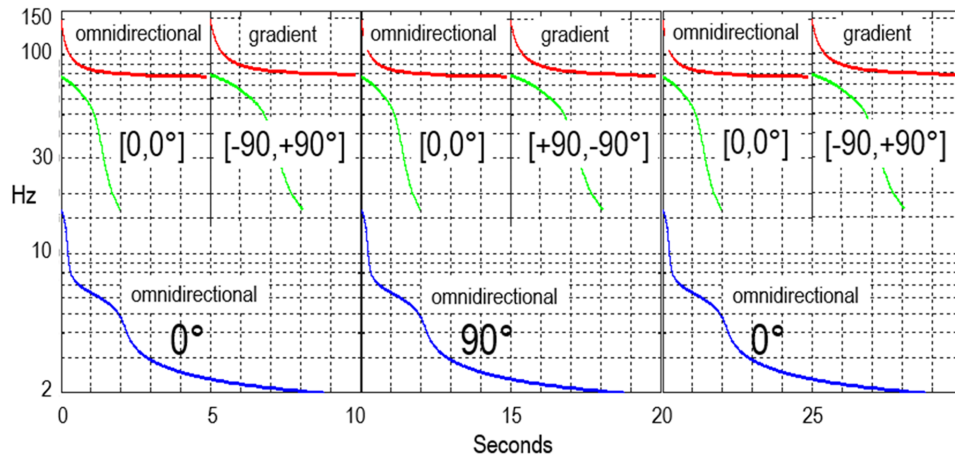
Figure 12 Example sweep sequence for OBN acquisition. Above 15 Hz the output alternates between conventional and transverse gradient sweeps. Below 15 Hz the gradient sweeps are not needed. Red group 1 at 9.5 m, green group 2 at 9 m, blue group 3 at 30 m depth.

the illumination requirements differ slightly (a transverse gradient source is less powerful acoustically than its corresponding omnidirectional source). Often it is more convenient simply to use the same sweep function for both directivity patterns, as is the case in the examples considered later.

In this example, for operational reasons, a depth constraint of 8–30 m is chosen as a constraint on the optimization code used to design the sweeps. The use of different constraints will give different sweeps and deployment depths.

3.4 Frequency hopping

It has been mentioned that there is no need for a silent time for the vibrators; they typically all emit sound continuously. This means they need to 'hop' from the last frequency of the sweep back to the starting frequency. The conventional way to do this would be to apply a taper down at the end and a taper up at the start with the taper length being many cycles long (Bagaini 2008). However, if the lowest frequency is, say, 2 Hz then a 'many cycle' taper is in danger of using up the entire sweep time.

Fortunately, there is a solution to this for most types of marine vibrator. Much shorter tapers can be used provided they are optimized so as not to place the device outside its design envelope (the device limits of displacement, velocity, acceleration and jerk). Using optimization within this envelope, tapers can be designed that are a fraction of a cycle long and yet do not make impossible demands on the device. The short tapers needed at low frequencies can exploit the device capabilities that are present in order that it can emit high frequencies.

The ability to hop from one frequency to another also raises the possibility of designing sweeps that deliberately skip certain frequency bands. Such a sweep may be used to sacrifice the energy at one frequency to spend more time emitting energy at another frequency (e.g. at very low frequencies), relaxing the sweep requirements. In a simultaneous source setting, sources can skip different parts of the bandwidth, allowing frequencies from two sources to be interleaved. Simultaneous source separation would then be followed by a simple band-pass filter. Future developments may allow the missing frequencies to be reconstructed, allowing the full bandwidth to be recovered (Halliday *et al.* 2015b).

4 MODELLING AND PROCESSING THE OCEAN BOTTOM NODE SCENARIO WITHOUT NOISE OR PERTURBATIONS

Using the methods described in the previous section, a marine vibrator ocean bottom node (OBN) acquisition scenario has been designed to replicate the processing results of a baseline airgun survey. The baseline survey is based on a deep-water OBN survey acquired offshore Nigeria (Chou *et al.* 2010). In this survey, a single source swath consisted of 13 lines of airgun source activations, with an in-line spacing of 30 m, and a sail-line move-up of 30 m. The 30 m grid of sources is interpolated on to a 15 m × 15 m source grid using a single-component matching pursuit approach (e.g. Schonewille, Klaedtke and Vigner 2009). This single-source swath takes a total time of 36 hours to acquire. While the source swath is being acquired, a node vessel is collecting and

re-deploying the outermost line of nodes. The time to collect and re-deploy the nodes is 22 hours, resulting in a shooting bottleneck.

The marine vibrator scenario uses a 90 m sail-line move-up. Along each sail line, the source array alternates between emitting wavefields with the two different types of directivity pattern illustrated in Fig. 11. The alternating sweeps are spaced at 15 m along each line. The 15 m × 90 m source grid is then interpolated on to the same 15 m × 15 m grid as the baseline airgun survey by a method we refer to as the "joint processing framework" (JPF), which is described next. Data quality is retained by the JPF because the additional gradient sweeps allow the data to be interpolated in the crossline direction using beyond-Nyquist reconstruction methods similar to generalized matching pursuit (Özbek *et al.* 2010; Vassallo *et al.* 2010). This interpolation then enables three-dimensional (3D) common node gather processing, as is typically used for deep-water OBN data.

By increasing the sail-line move-up in this way, the time to acquire a source swath is reduced from 36 hours to 12 hours. Thus, the shooting bottleneck is removed and the limiting factor is now the time to collect and re-deploy the nodes. Using two node vessels, reducing the time to collect and re-deploy nodes to 11 hours, the same survey can be acquired in one third of the time it would have taken with an airgun source.

4.1 Modelled acquisition effects

The data for the marine vibrator scenario are first modelled along densely sampled lines using 3D finite difference modelling. The SEAM (Society of Exploration Geophysicists (SEG) Advanced Modelling, www.seg.org/seam) Phase 1 model is used. A 20 km × 12 km portion of the model (away from the main salt body) is selected, and the seabed is around 1900 m depth. Nodes are placed just above the seabed, and pressure and particle velocity are modelled to enable up–down decomposition as part of the processing sequence.

For each node three datasets are modelled: one for the marine vibrator scenario, one for the equivalent airgun scenario, and one for the true reference (the directly modelled data on a 15 m × 15 m source grid). The desired geometries for each are plotted in Fig. 13(a–c). The extent of the source coverage for each node is 7.8 km × 7.8 km, and data will be modelled for 140 nodes (five lines of 28 nodes, on a 390-by-390 m grid).

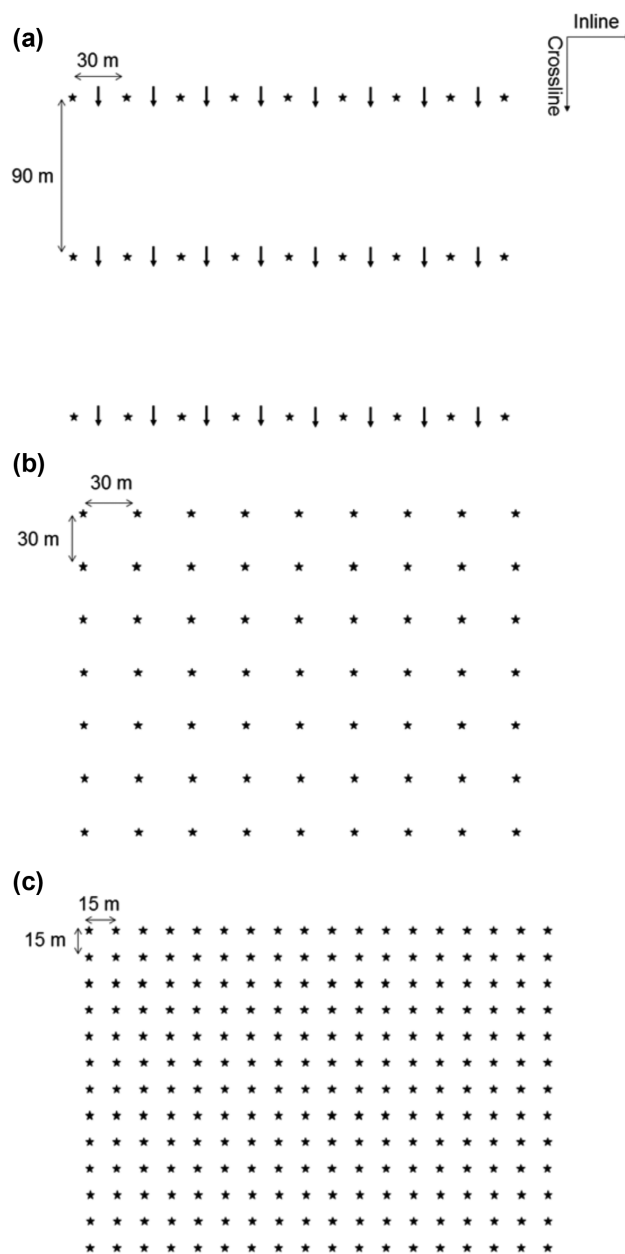For the marine vibrator, there are three source elements within the source array. A low-band element emitting 3–17

Figure 13 (a) Sketch of the geometry used for the marine vibrator OBN scenario. Stars indicate omnidirectional source points, arrows indicate directive (gradient) sources. (b) Sketch of the geometry used for the baseline airgun acquisition scenario. Stars indicated airgun source activation points. (c) Desired processed output from the geometries in both (a) and (b). Stars indicate impulsive (omnidirectional) source positions.

Hz is placed at 30 m depth and two high-band elements emitting 17–50 Hz are placed at 9 m depth with a separation of 15 m in the crossline direction. Here, the maximum frequency of interest will be 50 Hz. If higher frequencies were

of interest, then a third depth level would be introduced. The optimized sweeps in Fig. 12 are used here (with the gradient source using the same sweep function as the omnidirectional source).

Thus, for the marine vibrator scenario, three lines of densely sampled point sources are modelled for each pass of the source vessel, one corresponding to the low-frequency unit, and another two corresponding to the two mid-frequency units. These densely sampled lines are then used to construct the synthetic marine vibrator dataset, containing acquisition effects such as source motion and residual source noise (RSN).

Modelling the airgun baseline and the true reference datasets is more straightforward, as there are less acquisition effects to consider. For the airgun baseline sources are modelled on a 30 m × 30 m grid. At each source point, two source elements are separated by 15 m in the crossline direction to simulate the crossline extent of an airgun array. For the true reference dataset, point sources are modelled on a 15 m × 15 m grid. These datasets are also modelled to a maximum frequency of 50 Hz resulting in an alias-free reference dataset.

One of the key aspects of the marine vibrator acquisition scenario is the ability to control the source array to produce output wavefields with different directivity. In this report, the data are modelled to represent the data that would have been acquired if the marine vibrator emitted an omnidirectional wavefield and a transverse source gradient wavefield (Fig. 11). For this scenario, the alternating wavefields will allow alias-free data to be reconstructed from 90 to 15 m in the crossline direction. Ninety metre is six times the Nyquist sampling required for a maximum frequency of 50 Hz and a minimum velocity of 1500 m/s.

The low-frequency source only emits an omnidirectional wavefield. At 17 Hz, the edge of the signal cone (±1500 m/s) corresponds to a spatial Nyquist interval of 45 m; thus, two times Nyquist reconstruction is required across the 90 m crossline source gap. Note that the airgun baseline is acquired at 30 m, which is equivalent to twice Nyquist at the maximum frequency of 50 Hz. Since the goal of the airgun baseline is to reconstruct the source points from 30 to 15 m, we assume that performing twice Nyquist reconstruction *without* gradient sources is acceptable.

While the benchmark airgun source interval is 30 m, in the marine vibrator scenario the units emit a pair of alternating omnidirectional and gradient sweeps over the same 30 m interval. Thus, with the same vessel speed, this means that the time interval between sweeps is reduced, and the RSN experienced will be higher.

For the marine vibrator scenario, the RSN is created by the alternate directivity pattern. Thus, for the omnidirectional data the RSN is predominately caused by the directive sweep, and for the data of the directive sweep the RSN is predominately caused by the omnidirectional sweep. The patterns of phase in Fig. 12 allow the RSN to be separated using *f-k* methods, or alternatively, within the JPF described next.

When acquiring seismic data with an airgun array, the airgun releases the majority of its energy instantaneously at each source point. The marine vibrator will emit a sweep function, and the vibrator will sweep continuously. This means that the vibrator array will continuously emit energy as it moves between two nominal source points (the spatial locations corresponding to the sweep start times). This means that the vibrator is emitting energy as a function of time and space.

Hampson and Jakubwicz (1995) define the effective source signature, $S_{eff}(t, x)$, of a moving source as

$$S_{eff}\ (t,\ x) = S(t)\delta(x_0 + u_s t). \tag{2}$$

Here, $S(t)$ is the source signature, x_0 is the nominal source location, and u_s is the velocity of the source vessel. Thus, the delta function $\delta(x_0+u_s t)$ describes the motion of the source away from the nominal source location. For each time t, the output of the source at that time occurs at the position defined by $(x_0 + u_s t)$. Thus, the motion of the source can be modelled by interpolating each marine vibrator sail line on to a dense grid of points (where the sampling is equal to $u_s\Delta t$ with Δt equal to the sampling interval), and for each time sample t in $S(t)$ convolving that time sample with the corresponding point source at $(x_0 + u_s t)$.

For a vessel speed of 3 m/s and a time interval of 0.008 second, $u_s\Delta t$ corresponds to 0.024 m. Thus, to model the data as described above requires interpolation on to a very fine grid (e.g. over 1000 positions must be interpolated between nominal source points sampled at 30 m). The value 0.024 m is significantly less than the Fresnel zone of the frequencies of interest. It can be demonstrated that it is possible to relax this interval, without compromising the modelling results. To do this, rather than interpolating to a sampling of $u_s\Delta t$, a coarser sampling Δx is used. Rather than convolving single time samples with the corresponding point source, the sweep is split into a series of overlapping triangular windows (such that the sum of all overlapping windows is exactly the sweep prior to windowing). Each of the windowed sweep segments is convolved with the point source corresponding to the spatial location at the centre of the triangular window. Provided Δx is chosen carefully, this can produce equivalent

results to those using equation (2). Here we found that a value of 0.5 m was sufficient.

A continuous record is created for each of the three source elements separately. The wavefield recorded at the OBN is modelled for the first source, including the phase required for the directional output and for RSN control, and the source motion. The equivalent wavefield for the next sweep is modelled, and is added to the wavefield for the first sweep, but delayed by the time corresponding to the sweep repetition interval. In this way, the RSN is naturally included in the modelled continuous record. This is repeated until the entire continuous source line has been modelled. The alternating direction of the source vessel is considered when modelling the RSN and the source motion.

Once the three continuous records have been produced they are summed together. When those for the mid-band sources are summed, the alternating omnidirectional and directive sources are created (since the corresponding phase was already included). The continuous records are sorted into common node gathers by aligning the data to the start times and the phase of the desired source.

4.2 Joint processing framework

In general, methods to remove or account for acquisition effects in seismic data are applied in a certain data domain (common source gather, common receiver gather, common offset gather and so on), and require some model of the underlying wavefield. Many methods use some form of transform domain to describe this model. For example, this transform domain could be the frequency-slowness domain (Moore *et al.* 2008; Özbek *et al.* 2010), tau-*p* domain (Schonewille, Dishberger and Kapadia 2014), curvelet domain (Herrmann *et al.* 2008) and so on. Each element in this domain may be referred to as a 'basis function', and each of these basis functions represents one particular model that contributes to the description of the data. The choice of transform domain is dictated by the particular acquisition related effect being accounted for. It must be possible for the acquisition effect to be described using the basis functions (or by some linear combination of basis functions), but it must also be possible for the desired data (without the acquisition effect) to be described using the same basis functions. The method may then operate by matching the input data to the basis functions describing the input data. This provides an underlying model, which when combined with the equivalent basis functions describing the desired output data, gives the output data with the acquisition effect removed.

Here the case where multiple acquisition effects are dealt with simultaneously is considered. The requirements for this are that the multiple acquisition effects must be observed/explained in the same data domain, and that the multiple acquisition effects can be modelled/removed using the same basis functions.

One such existing method of joint processing is Generalized Matching Pursuit (GMP), a joint interpolation and deghosting method described by Özbek *et al.* (2010). In GMP, the receiver-side ghost is removed from the data, and the data are simultaneously interpolated on to a dense grid of receiver positions using carefully chosen basis functions and a model for the ghost.

The source situation is different, as here the aim is to correct for data acquisition effects on the source side introduced using a marine seismic vibrator, such as source motion correction, source signature removal, RSN attenuation and source-side reconstruction and regularization. The source signature term can include the directional part of the signature, including any imposed source directivity as well as the source ghost term.

For the current marine vibrator scenario, the source data are recorded by OBN. In this case, each of the data effects can be fully observed and described in the common node gather data domain. This data domain is a 3D gather (frequency, and two spatial source coordinates, *f-x-y*). A suitable transform domain is then the frequency-slowness (f-p_x-p_y) transform. The acquisition effects can then be described as follows.

- The source signature is described as a 3D radiation pattern $S(f, p_x, p_y)$; this term includes the directivity of the source wavefield. This is described by the farfield radiation pattern (see Hopperstad, Laws and Kragh 2008, for a description of the farfield radiation pattern).
- The alternating directivity patterns can be included by defining a spatially varying radiation pattern for each nominal source with coordinates x and y: $S(f, x, y, p_x, p_y)$.
- If the marine vibrator source has a linear sweep, then source motion is dependent on frequency, source position and slowness. If the motion is in the x direction, and the deviation from the true source position for frequency f is Δx_f, the motion can be described with a term $M(f, x + \Delta x_f, y, p_x, p_y)$.
- The reconstruction and regularization problem aims to find the model components describing the acquired data, for example using basis functions $D(f, x, y, p_x, p_y)$ that incorporate the acquisition effects. These components are then used to model data on a desired output grid, for example

using basis functions $D(f, x^d, y^d, p_x, p_y)$, where x^d and y^d are the desired output coordinates.

- The RSN is dealt with in a similar way, but with a corresponding phase term used to describe the phase-sequence encoding, for example $D^{rsn}(f, x, y, p_x, p_y, \varphi)$.

Thus, each of the effects to be accounted for is dependent on combinations of the source x and y coordinates, frequency and the slowness in x and y directions. While each of these effects can be solved separately, this scenario meets the two requirements for the JPF that (1) each of the effects can be observed/described in the same data domain (the common node gather), and (2) that each of the effects can be described in the same transform domain (the f-p_x-p_y domain). It is therefore possible to solve this set of problems in a single joint processing step.

While the description here is for the case of OBN acquisition, a similar processing framework could also be envisaged for the towed streamer scenario. However, whereas for OBN acquisition there is a single fixed receiver recording data from many sources distributed in the in-line and crossline direction, in towed streamer acquisition there are no fixed receivers, and typically the receivers will only record sources distributed (predominantly) in the in-line direction. This means that the receiver motion must be accounted for, and that the ability to deal with crossline source effects can be more challenging (whether it is reconstruction of the wavefield, or accounting for the crossline ghost effect).

4.3 Reconstructing the OBN data

The JPF is now demonstrated using the modelled OBN acquisition scenario. First, the sweeps are deconvolved from the respective parts of the data, as this makes time windowing of the data easier. Next the JPF is applied to data in overlapping time windows of 0.5 second, and overlapping spatial windows of 180 m × 180 m.

Figure 14 shows the reconstruction result for a central crossline through the common node gather. Figure 14(a) shows the input marine vibrator data. Note that the data are plotted with five of six traces containing no data (the empty traces are those that will be reconstructed). Figure 14(b) shows the equivalent airgun data, with one of two traces containing no data, and Fig. 14(c) shows the reference, which has data in every trace. Corresponding *f-k* spectra are shown in Fig. 15(a–c). Note that there is a small gap in the marine vibrator data in Fig. 15(a). This is because in this modelling study no overlap exists between the two different emitted band-

widths, tapers are applied at the edge of the bands during deconvolution.

The processing results for each of Fig. 14(a–c) are shown in Fig. 14(d–f). A multi-frequency constraint has been used to ensure that the solution at one frequency does not differ significantly from the solutions at neighbouring frequencies. Despite requiring reconstruction from 90 to 15 m, the marine vibrator scenario produces comparable results to the airgun scenario (requiring three times as much acquisition time) and to the true reference data. The airgun scenario reconstruction using a single-component matching pursuit algorithm also removes the source ghost effect, and this same effect has also been removed from the true reference data to allow a direct comparison.

The *f-k* spectra are shown in Fig. 15(d–f). The input marine vibrator data in Fig. 15(a) have six overlapping copies of the data (the true wavefield and five aliased replicas), and the JPF has been able to successfully identify which parts of the data correspond to the true wavefield (Fig. 15d). An L1 deconvolution method has been used to remove the gap between the two bandwidths for the marine vibrator data (Beck and Teboulle 2009). The RMS errors in Fig. 15(d–e; with reference to Fig. 15f) are −22.5 and −29.6 dB, respectively.

To illustrate the 3D nature of the wavefields, a number of time slices are plotted in Fig. 16. Figure 16(a) shows the reconstructed marine vibrator scenario, Fig. 16(b) the reconstructed airgun scenario, and Fig. 16(c) the true reference. The reconstruction errors for the vibrator and the airgun are shown in Fig. 16(d,e), respectively. These difference plots indicate that the JPF gives excellent results for the marine vibrator data, and that these compare favourably with the reconstruction of the baseline airgun scenario. These results are plotted with the frequency gap shown in Fig. 15(a) present in the marine vibrator data (i.e. no L1-deconvolution was used here), and for a direct comparison, the same gap is introduced into the airgun baseline data, and the true reference. This has been done despite being shown above that it is possible to deal with this gap in processing, as this was applied as a post-processing step, and not during the reconstruction itself. This means that for this small range of frequencies, the error is higher than at other frequencies. This increased error is not related to the reconstruction but is a consequence of modelling the scenario with a small gap between the two vibrator bandwidths. To give a fair comparison of the reconstruction, the gap is introduced into the airgun and reference. The RMS errors (relative to Fig. 16c) in Fig. 16(d,e) are −27.7 and −27.5 dB, respectively. Note that the gap exists because of the way the data
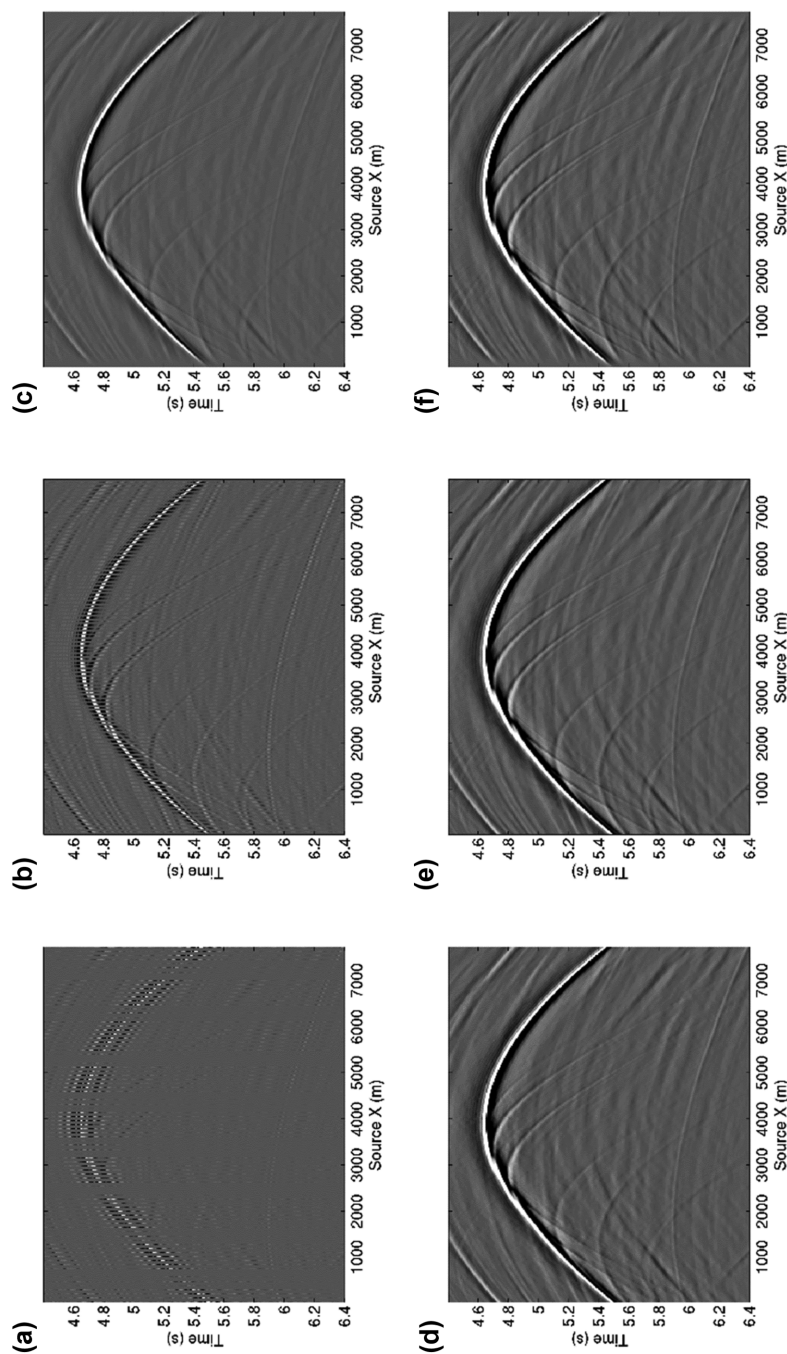
Figure 14 Crossline slices of the input common node gather for (a) the marine vibrator scenario, (b) airgun baseline scenario, and (c) true reference data. (d) Output of the joint processing framework for the marine vibrator. (e) Equivalent reconstructed data for the airgun baseline. (f) The equivalent processed output for the airgun baseline. (f) The equivalent processed output for the true reference data. Note that the data are plotted with the same number of traces, thus five of six traces are empty in (a) and one of two traces are empty in (b). The error in (d) compared to (f) is −22.5 dB, and the error in (e) compared to (f) is −29.6 dB.
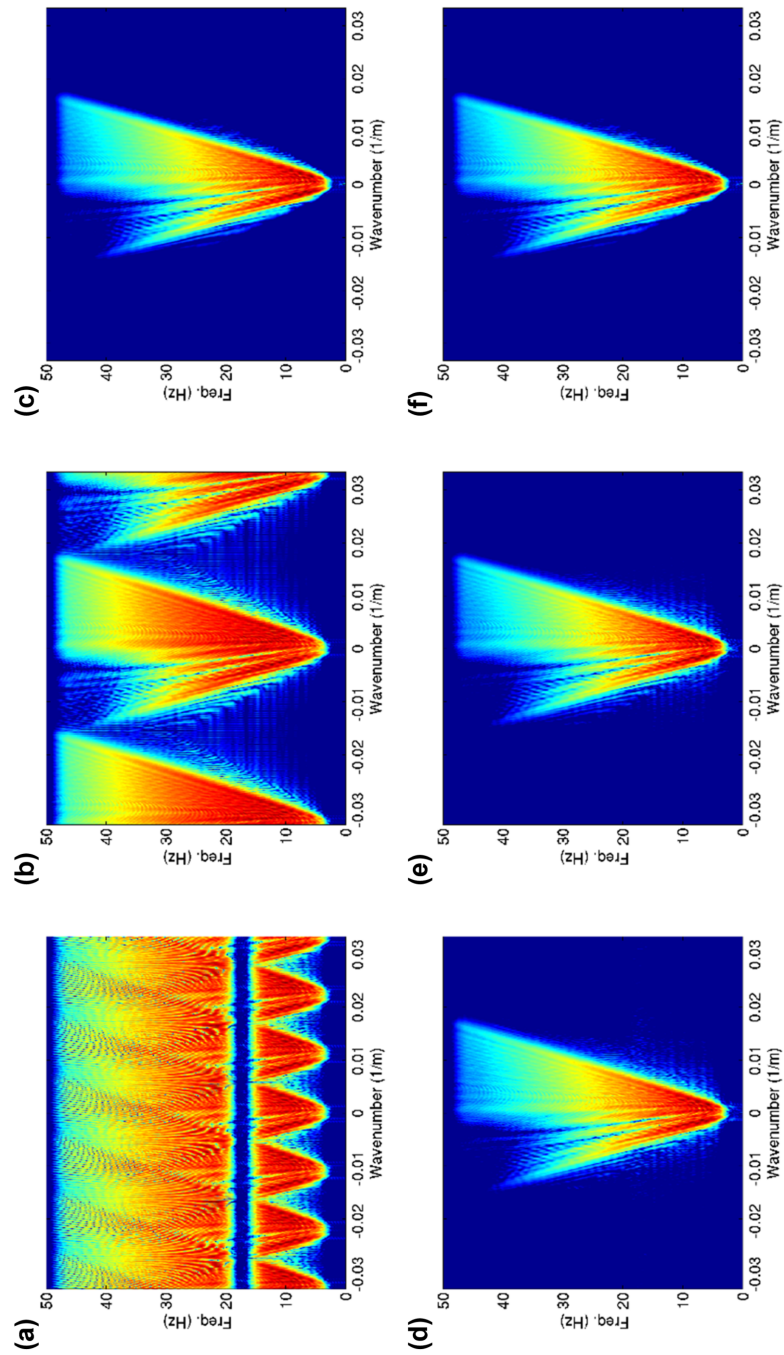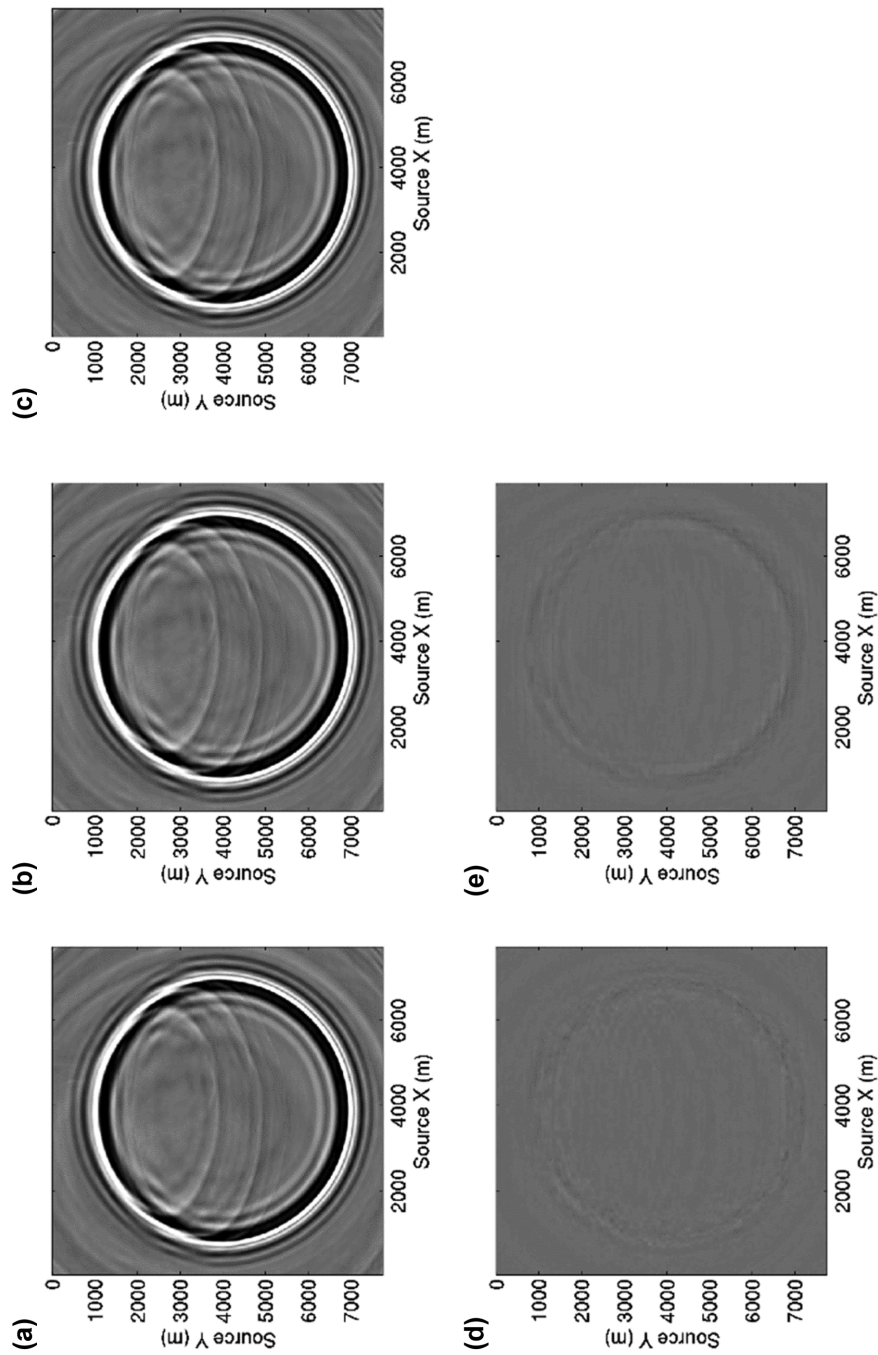
Figure 15 Frequency–wavenumber spectra of the data plotted in Fig. 14.

Figure 16 Time slices (*T* = 5 seconds) from an OBN gather for (a) the joint processed marine vibrator data, (b) the reconstructed airgun baseline data and (c) the true reference. Subparts (d) and (e) show the difference between (a) and (c), and (b) and (c), respectively. The RMS error for the time slices in (d) and (e) compared with the data in (c) are −27.7 and −27.5 dB, respectively.
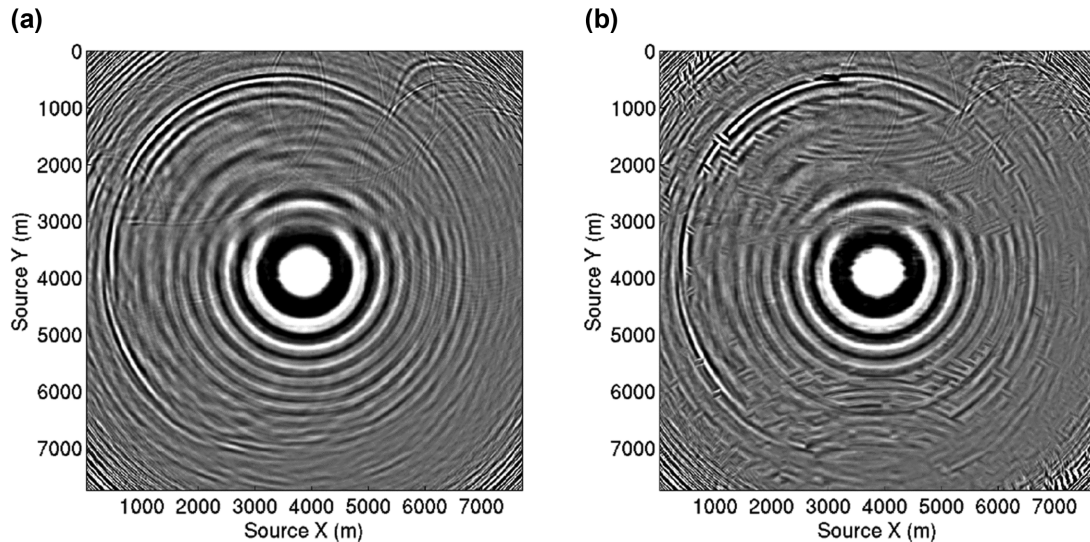
(a)

(b)

Figure 17 Time slices ($T = 4.6$ seconds) from an OBN gather for the joint processed marine vibrator data with (a) all acquisition effects account for and (b) with all acquisition effects accounted for, but where the contribution of the directive source is set to 0.

were modelled, and not because of any limitation with hardware design or processing capabilities.

Another time slice is shown in Fig. 17. In Fig. 17(a) a reconstructed time slice from the marine vibrator scenario is shown, where all acquisition effects are accounted for. In Fig. 17(b) the same time slice is shown, but where the contribution of the gradient source is set equal to zero. In this case, there are many events that are not reconstructed correctly; the data quality has been compromised. This result indicates the added value of the transverse gradient source in obtaining information away from the sail line.

4.4 Further processing

To demonstrate fully the proposed marine vibrator scenario, the data are further processed through to a migrated image. This is done for all three datasets, so that a comparison of the data at the final stage of processing can be made. The workflow follows that of a typical deep-water OBN flow (e.g. Kristiansen *et al.* 2014). For the marine vibrator and airgun baseline scenarios, the reconstruction is performed for both pressure and particle velocity for each of the 140 nodes. These components are reconstructed simultaneously, and the reconstructed particle velocity is scaled appropriately during the reconstruction such that up–down separation can be performed by a simple summation or subtraction after reconstruction. These two reconstructed components are then separated into up- and down-going wavefields, and an up–down deconvolution is performed in the frequency-wavenumber (f-k_x-k_y)

domain to remove the free-surface-related multiples. These multiple-free data are then migrated to give a 3D migrated volume. Note that the down-going wavefield can also be used for mirror migration, but this result will not be shown here. The true reference data are also migrated. This is done after wavefield separation and up–down demultiple are performed in the f-k_x-k_y domain and followed by reverse time migration (RTM).

Figure 18 shows the part of the migrated volume directly beneath the central line of nodes. Fig. 18(a) shows the migrated data for the marine vibrator scenario, Fig. 18(b) for the airgun baseline, and Fig. 18(c) for the true reference. The two scenarios produce migrated images that are of a very similar quality to the true reference, the RMS error for the marine vibrator scenario is -25 dB, whereas for the airgun scenario it is -29 dB.

5   PERTURBATIONS AND TOLERANCES

The modelling and processing considered in the previous section were for the case where the survey was acquired as expected; no perturbations or noise were included. To define hardware tolerances, it is important to assess how the different perturbations and sources of noise, introduced during acquisition, will affect our ability to acquire and process the data. Acquisition related perturbations that have been studied include
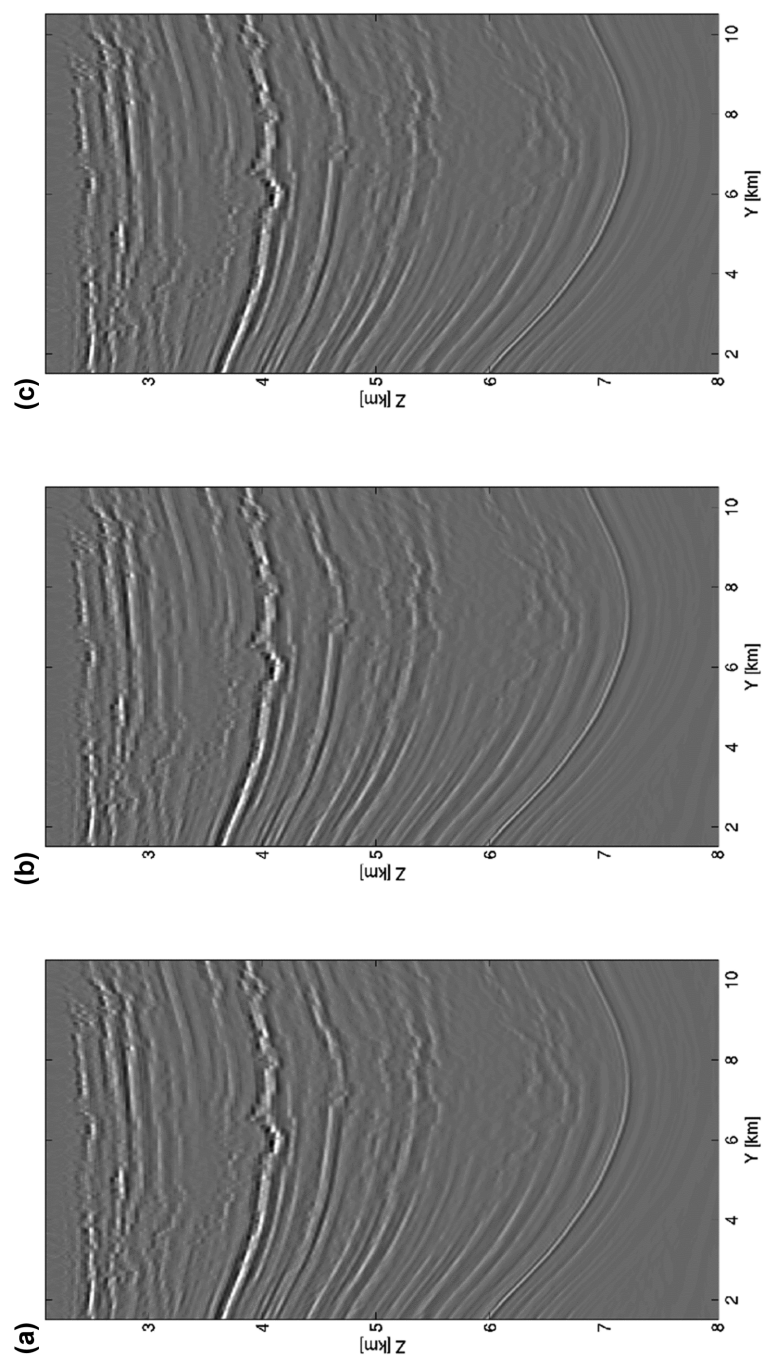
- the impact of ambient and system-generated noise;

Figure 18 Crossline slices through the RTM images for (a) the marine vibrator scenario, (b) the airgun baseline scenario, and (c) the true reference.

- the impact of position errors (i.e. when we did not put the source where we wanted, but we were able to measure where it was);
- the impact of position measurement errors (where there is uncertainty in the measured position);
- the impact of a rough sea surface.

The full analysis of each of these perturbations is beyond the scope of this paper. Instead we briefly consider each effect in turn and give an example of the change in the processed results that can be expected as a result of perturbations. The level of the modelled perturbations was chosen to match the expected tolerances of the hardware system.

5.1 Ambient and system-generated noise

In the second section of this paper, the design of sweep functions based on desired image signal to noise was discussed. These sweeps ensure that the emitted signal is sufficient to overcome the noise observed in the image. However, when considering the pre-imaging processing of the data it is the noise observed at the gather level that is important. Many modern seismic processing methods, such as the matching pursuit approach used to reconstruct the data in this paper, are strongly data-dependent. These methods typically involve some sort of integral transform (e.g. a slowness transform) summing data from different source locations. Since the observed noise will vary from sweep to sweep it will be suppressed somewhat during the reconstruction process. To assess this, real noise from an ocean bottom dataset (appropriately scaled to match the finite difference amplitudes) can be added to the synthetic data. Halliday *et al.* (2015a) considered data from a special noise test that allowed both ambient noise, and system (source vessel) generated noise.

This dataset provides both ambient and system-generated noise that can be added to the synthetic data. As an example, for a window of data from 5.75 to 6.25 seconds, the added noise is around 20 dB lower than the signal. However, since this is real noise, there are regions where the noise is strong, for example where there are bursts of noise.

5.2 Positioning errors and positioning measurement errors

Seismic data acquired by the marine vibrator will be affected by the waves on the sea surface and this will, in turn, affect the reconstruction. The sea surface moves and the source will be dragged through the moving currents beneath the surface. There are two consequences of this: one is that the reflection of sound from the sea surface is complicated because of the non-flatness; the other is that the motion of the source through the water is complicated because of the hydrodynamic forces that act upon it. When the vibrator array configuration moves away from the planned positions, these positions must be measured. There are two distinct considerations here: the first is the effect of *known* positional perturbations on the processing of the data; the second is the effect of error in the measurement of those positions.

The dynamic behaviour of a marine vibrator towing system in the presence of sea surface waves and currents was simulated using the AquaSim software package. The positional variations of individual vibrator units were then used in the modelling of the impact of positional perturbations on synthetic seismic data. Thus, these positional perturbations are representative of those that would be observed when acquiring data in a rough sea with a significant wave height of 4 m. Figure 19 shows an example of the simulated positions during a single 10-second sweep, for a low-frequency (3–17 Hz) vibrator with a nominal deployment depth of 30 m. Figure 19(a) shows positions in the horizontal (*X–Y*) plane, Fig. 19(b) shows the positions in the *Y–Z* plane and Fig. 19(c) shows the position in the *X–Z* plane (in black). Note that the position in the *X–Y* plane appears to be stable, but there is much more variation of the source position with depth (*Z*). The variation with depth can have a more significant effect on the marine vibrator data because it will change the nature of the ghost response that affects the down-going wavefield.

Provided the positions are known, the variations are expected to have a small effect on the reconstruction of the data. These variations introduce a degree of non-uniformity into the data, which could be expected to aid in the reconstruction process (Mosher *et al.* 2014). The requirement to know the perturbed positions places a constraint not only on the accuracy of the sensors being used to measure those positions, but also on the update rate of those positions (since the time-varying position of the source, while it emits the swept waveform, needs to be known).

5.3 Rough sea effects

The rough sea effect is introduced due to the non-flatness of the sea surface. Using the same sea surface waves as those considered in the study of positional variations, we can model the impact of the rough sea effect on the synthetic marine vibrator data, allowing the impact on the reconstruction process to be investigated. The time-varying sea surface and its time-varying
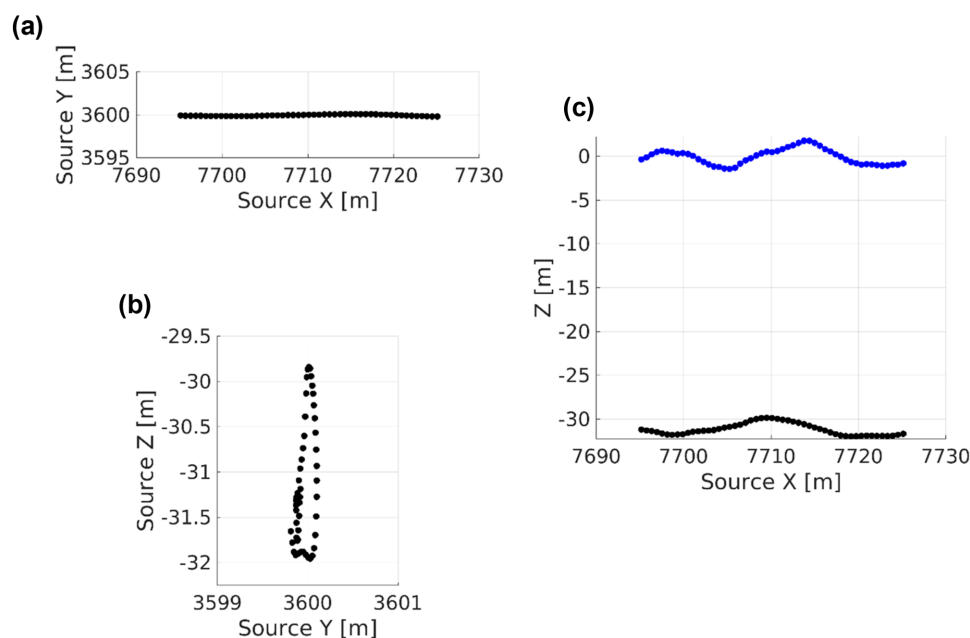
Figure 19 Positions occupied by a low-frequency marine vibrator during one 10-second sweep are plotted in black for (a) the horizontal (*X*–*Z*) plane, (b) in the *Y*–*Z* plane, and (c) the *X*–*Z* plane. The sea surface above the source is plotted in blue in (c).

scattering response are generated using the method given by Laws and Kragh (2002).

The reconstruction approach used in this paper assumes that the local sea-surface is flat and horizontal. There are two approximations for describing its height to the reconstruction algorithm. In the simpler approximation, it can be assumed to lie at mean sea level; in the more advanced approximation it can be assumed to lie at the height of the sea directly above the source (a quantity that is easy to measure). Neither of these approximations accounts properly for the scattering of acoustic waves by the rough sea waves, but this is fully included in the forward modelling.

In Fig. 19(c), the sea height above the modelled marine vibrator positions is plotted in blue. Note that the source position variation in depth (in black) does not directly correspond to the sea height. This is because the simulation of the towing system does not assume that the vibrator elements are buoyed as would be the case with an airgun source (see Laws and Kragh 2002). This means that we cannot assume that the source stays a fixed depth below the local sea surface.

The vertical incidence rough sea ghost responses that correspond to each of the positions in Fig. 19 are plotted in Fig. 20(a). The expected location of the first and second ghost notches based on the sum of the module depth and the local sea height (i.e. the distance between blue and black po-

sitions in Fig. 19c) is plotted as the dashed white line. This dashed line corresponds to the approximation that there is a flat sea surface, with the height of the surface varying as the height of the sea directly above the source. Although the dashed line does not exactly match the observed notch positions of the three-dimensional (3D) rough sea response, it is a much closer fit than would be obtained using a fixed height, flat sea surface (the notches for this would plot as horizontal lines).

We also show the amplitude emitted by the moving marine vibrator under the rough sea surface, for example a low-band sweep, in Fig. 20(b) (overlapping triangular windows are used to split the sweep into parts with each part emitted at each time and position occupied by the vibrator). The dashed line indicates the swept frequency as a function of time and position. By comparing Fig. 20(a) and Fig. 20(b) we can see that even with the rough sea effect, the ghost notch does not enter the bandwidth emitted by the marine vibrator. This means that we avoid the notch frequencies where the rough sea effect is at its largest (Laws and Kragh 2002); it is not possible to do this with an airgun source. Thus, we might expect a marine vibrator deployed in this way to be less sensitive to a rough sea than an airgun source would be. The amplitude variation will still affect the output, as will the scattering effect (which is not obvious in an amplitude display), but the impact of these is expected to be smaller.
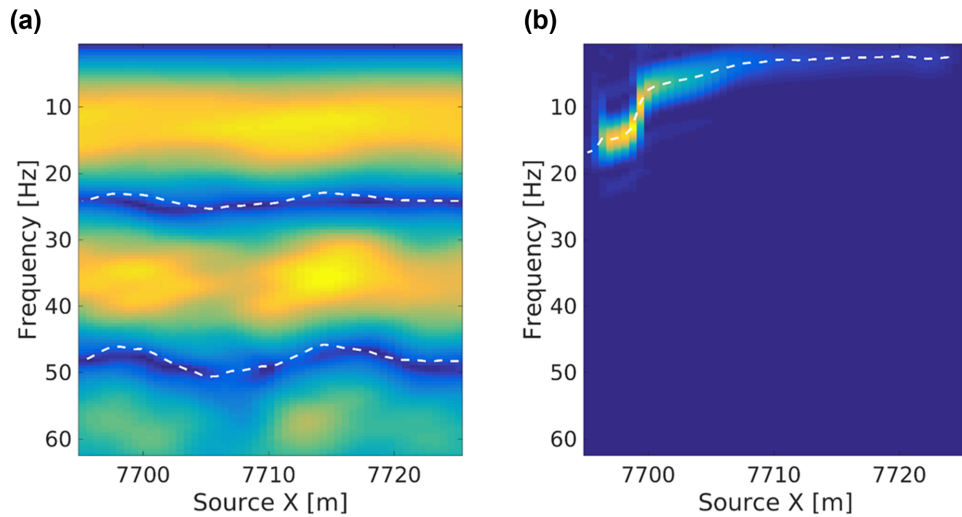
Figure 20 (a) The amplitude of the rough sea ghost response, computed for vertical incidence, for each of the positions occupied by the marine vibrator in Fig. 19. The location of the ghost notches computed using the sum of source *z*-coordinate and local sea height are plotted as white dashed lines. (b) The amplitude spectra of the part of the sweep function emitted at each spatial location. The sweep frequency as a function of time/position is plotted as the dashed white line.
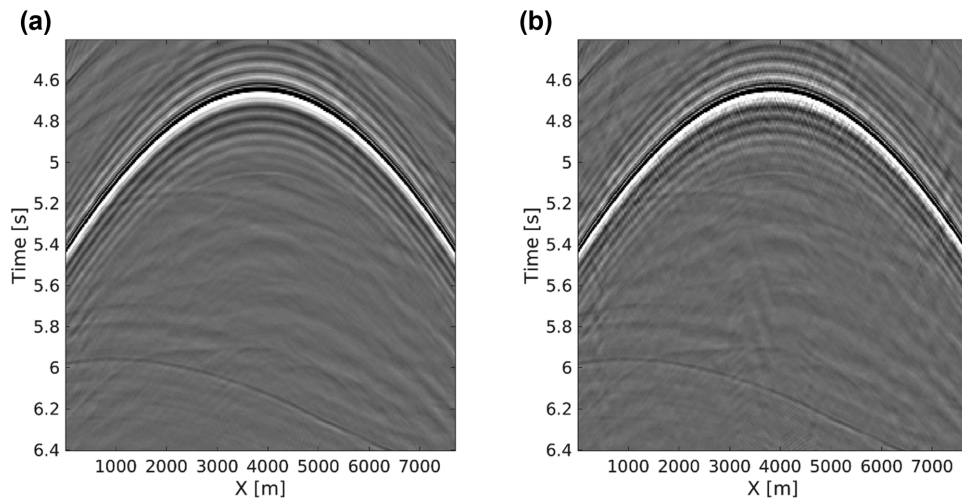
Figure 21 Reconstruction of a source line, where there are (a) no perturbations in the modelled data, and (b) where ambient and system noise, positional perturbations and the rough sea effect are included in the modelled data. Positional perturbations are assumed to be known, and the local sea height is used to correct for the rough sea effect.

5.4 Reconstruction of perturbed data

We now consider the reconstruction of the data that have been modelled including the three effects described above. Figure 21(a) demonstrates the reconstruction of data without any perturbations in the modelled data. This result is very similar to the results in the third section of this paper, but here uses a different modelling workflow that has been designed to allow the positional perturbations, and the rough sea effect to be included in the modelling of the data. The angle-dependent

ghost operators for this rough sea are introduced into the synthetic data using a local 3D (*t*, *x*, *y*) convolution operator. Figure 21(b) shows the same reconstruction result but for the case where ambient noise, positional perturbations and the rough sea effect have been included in the modelling.

Due to instabilities in the rough sea modelling at higher take-off angles, here we have limited the take-off angles to 60° for both unperturbed and perturbed cases. The results here also differ from those in Fig. 14, as in this comparison,

the L1 deconvolution step has not been used to fill in the gaps in the bandwidth.

The modelled rough sea has a significant wave height of 4 m (typically the highest sea marine seismic data would be acquired in Laws and Kragh (2002)). In this case, the positional perturbations are assumed known, and the local sea height above each vibrator module is used to help correct for the rough sea effect. While the reconstruction of the data with perturbations does appear noisier, this is expected when comparing with the noise-free, ideal situation. The difference between these two reconstructed datasets represents the perturbation noise. For the data shown in Fig. 21, the signal-to-perturbation noise ratio is 20–22 dB for the low-band source and 15–17 dB for the mid-band source. Laws and Kragh (2002) found that, for the case of a buoyed airgun in a sea with a 4 m significant wave height, the rough sea effect alone (with no perturbations, ambient noise or reconstruction of the data) gave a signal-to-noise ratio (SNR) of around 16.5 dB. This suggests that the effect of the rough sea effect on the marine vibrator data considered here is of a similar magnitude to that for an airgun survey.

Other important perturbations or sources of noise, which are not considered here, relate to the ability to emit a desired waveform, as well as the ability to measure that emitted waveform. This includes the impact of distortion of the output waveform, errors in the phase of the output waveform and perturbations in the sensors that measure those waveforms.

6 THE PROTOTYPE VIBRATOR

A prototype vibrator (Fig. 22), designed to meet the criteria defined by the methods described herein, has been built and tested. A more mature full-scale design is shown in Fig. 23. Each vibrator has two opposed radiators that move in and out and are connected to the housing by annular rubber boots. The overall volume of the unit changes as the radiators move and this is what causes the radiation of the sound.

Each vibrator element is designed to have a configurable core, so that it can be configured in the field to emit the frequency range required for any specific survey. The fluid flows around the device are modelled (Fig. 24) to aid the design of the internal electro-hydraulic drive, to design out any risk of cavitation and to characterize the acoustic signature.

The output waveform is determined using accelerometers mounted on the projector faces (Laws 2013). The notional source signature (Ziolkowski *et al.* 1982) depends on the second time-differential of the volume. For this to work accurately the flexing of the rubber boots (Fig. 25) must be

Figure 22 An early (2012) scaled-down prototype of the marine vibrator. A typical seismic array would include multiple units.
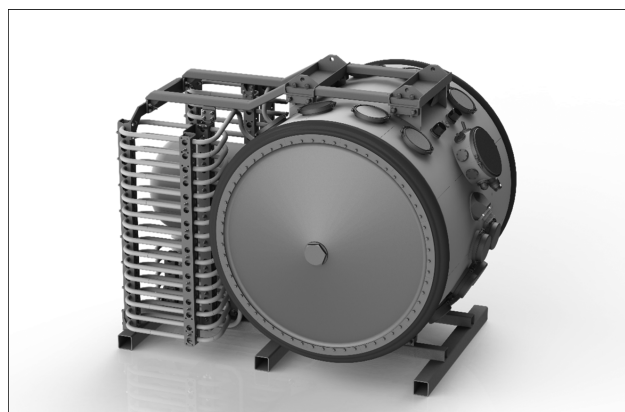

Figure 23 Each vibrator unit is a double ended 'drum' with the two projector faces attached to the 'drum' housing by two circular flexible rubber boots.

correctly included in the calculation. A closed-loop feedback control uses the measured waveform to control the actuators and thereby keep the distortion to a minimum.

To emit the acoustic signal, the vibrator requires infrastructure from a range of support subsystems such as control electronics, towing equipment, navigation devices, power supplies and handling systems. Advanced systems engineering
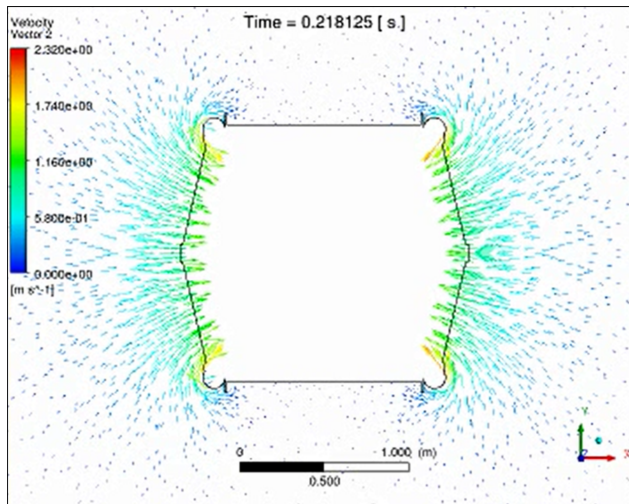
Figure 24 The fluid velocity is simulated around the vibrator unit. The small curved 'corners' are the flexible boots.

methods were applied to combine these subsystems into an integrated system that is optimized to support the geophysical needs described in the preceding sections. Model-based systems engineering methods and sophisticated physics-based

models were instrumental in designing and validating the complex interfaces, and optimizing system performance. To consolidate the system's designed-in safety and reliability, it is certifiable against the DNV GL rules for classification of underwater technology under DNV GL-RU-UWT.

7 ENVIRONMENTAL VALUE OF MARINE VIBRATORS

While the marine vibrator system presented in this paper focussed on geophysical benefits, ongoing research indicates that vibrators are less potentially damaging to marine animals than airguns are. Southall *et al.* (2007) defined two metrics that were closely related to disturbance and injury in marine mammals. The metrics are the peak pressure (PK) and the 24-hour hearing-weighted sound exposure level (SEL). These same two metrics were used by NOAA (2016) for marine mammals and were also adopted by Popper *et al.* (2014) in their provisional injury criteria for fish, fish eggs, fish larvae and sea turtles.

For marine mammals, most notably for the low-frequency cetaceans, the dominant metric is considered to
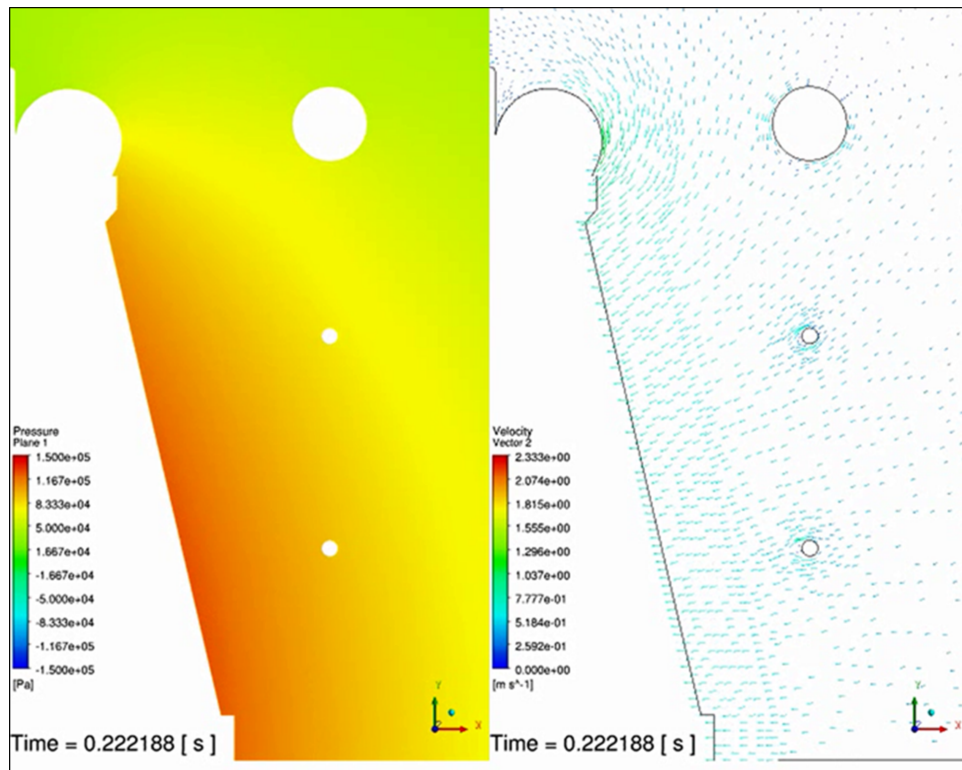

Figure 25 The shape of the flexible boot is modelled in detail so that the far-field pulse can be properly derived from accelerometers mounted on the projector faces.

be the SEL rather than PK. To an extent, mammal hearing adapts to the incoming sound to defend against injury, but it can only do this if the sound is 'nonpulsed', the term coined by Southall *et al.* (2007). As a result, the SEL injury threshold is higher (more robust) for non-pulsed sources than it is for pulsed sources. The sound from a marine vibrator is classed as non-pulsed, and it is therefore less likely to cause injury than the impulsive sound from an airgun even if the SEL is the same. For mammals, vibrators win over airguns because vibrators are non-pulsed.

According to Popper *et al.* (2014), for fish and sea turtles the situation is different. Adopting a precautionary principle, it is PK that is the dominant metric rather than SEL. This applies to all fish groups (with or without swim bladders), fish eggs, fish larvae and sea turtles. The criteria of Popper *et al.* (2014) are preliminary, and they might change when more data become available, but based on current criteria, for fish, vibrators win over airguns because their peak pressure is lower.

8   CONCLUSIONS

The efficiency of seismic surveying can be greatly improved using marine vibrators in place of airguns. In the example discussed herein, a deep-water ocean bottom node (OBN) survey could have been acquired using marine vibrators in one third of the time that it took using airguns.

To achieve this dramatic improvement in efficiency we use the vibrator's ability to emit a frequency sweep with an arbitrarily specified phase, which might depend on frequency. Using a sequence of phases, with the phase changing from sweep to sweep in a pre-defined sequence, we can attenuate residual source noise (RSN) and insert extra sweeps interleaved between the conventional sweeps. We use these extra sweeps to emit a horizontal gradient wavefield by running crossline-separated pairs of vibrators in antiphase. The same vibrators are run in phase for the conventional (omnidirectional) sweeps.

Processing the new marine vibrator sweep data does require a new processing method, referred to as the joint processing framework (JPF). This framework allows the handling of several acquisition effects in a single step. These can include source motion correction, sweep deconvolution, source deghosting, RSN removal, simultaneous source separation and wavefield reconstruction. All the significant source perturbations are removed and the data are reconstructed unaliased on a grid.

Realistic simulated OBN data, acquired with the marine vibrator data and processed in the JPF, produce an image with the same quality as one obtained in the conventional airgun survey, but the new method requires one third of the number of sail lines. Detailed simulation of the survey in three dimensions (3D), including noise and perturbations, has led to the design specification of the vibrators themselves, the deployment arrangements, the system that measures the positions, and the system that measures the emitted waveforms.

In addition to the efficiency advantages, the marine vibrator system described in this paper still offers the same environmental benefits as other marine vibrator systems. This is because the marine vibrator is a 'non-pulsed' source and is considered less intrusive to marine mammals as a result. In addition, it has a lower peak pressure than an airgun array and is less potentially injurious to fish as a result.

REFERENCES

Bagaini C. 2008. Low-frequency vibroseis data with maximum displacement sweeps. *The Leading Edge* **27**, 582–591.

Beck A. and Teboulle M. 2009. A fast iterative shrinkage-thresholding algorithm for linear inverse problems. *SIAM Journal on Imaging Sciences* **2**, 183–202.

Bird J.M., Peacock J.H. and Walker L.J. 1984. Development of a hydraulic transducer for marine seismic. 54th SEG annual international meeting, Atlanta, Expanded Abstracts, 825–826.

Chou T.G., Hicks D., Sydora L., Iyiola S., Nworah N. and Arowolo I. 2010. OBN (ocean bottom nodes) acquisition for reservoir management and surveillance at Agbami Field, Nigeria. 80th SEG annual international meeting, Houston, TX, Expanded Abstracts, 3756–3758.

Feltham A., Girard M., Jenkerson M., Nechayuk V., Griswold S., Henderson N. *et al.* 2017. The Marine Vibrator Joint Industry Project: four years on. *Exploration Geophysics* **49**, 675–687.

Haldorsen J., Desler J.F. and Chu D. 1985. Use of vibrators in a marine seismic source. 55th SEG annual international meeting, Expanded Abstracts, 509–511.

Halliday D.F., Laws R.M. and Garden M. 2015a. Signal and noise in a shallow-water ocean-bottom cable survey. 85th SEG annual

international meeting, New Orleans, Expanded Abstracts, 120–124.

Halliday D.F., Laws R.M., Hopperstad J.-F., Muyzert E. and Coste E. 2015b. *Frequency-sparse seismic data acquisition and processing*. US patent US20140278116A1.

Halliday D.F., Laws R.M., Özbek A. and Hopperstad J.-F. 2017. Separating simultaneous sources using phase-sequencing and reconstruction in marine seismic vibrators. 79th EAGE meeting, Paris, Expanded Abstracts, We-P3-15.

Halliday D.F. and Moore I. 2018. A comparison of random and periodic marine simultaneous-source encoding. *The Leading Edge* 37, 471a1–471a11.

Hampson G. and Jakubowicz H. 1995. The effect of source and receiver motion on seismic data. *Geophysical Prospecting* 43, 221–244.

Herrmann F.J., Wang D., Hennenfent G. and Moghaddam P.P. 2008. Curvelet-based seismic data processing: a multiscale and nonlinear approach. *Geophysics* 73, A1–A5.

Hopperstad J.-F., Laws R. and Kragh E. 2008. Where is the center of a multi-depth marine source array? 78th SEG annual international meeting, Las Vegas, Expanded Abstracts, 40–44.

Johnson G.R., Thompson I. and Walker L.J. 1988. The GECO marine vibrator system. 58th SEG annual international meeting, Las Vegas, Expanded Abstracts, 71–74.

Kragh E., Laws R.M., Hopperstad J.-F., Morgan G. and Kireev A. 2012. Reducing the size of the seismic source with a 4C towed marine streamer. 74th EAGE meeting, Copenhagen, Expanded Abstracts, Z014.

Kristiansen P., Ogunsakin A., Esotu M., Zdraveva O., Hootman B. and Quadt E. 2014. Deepwater OBN – exploiting data-processing possibilities. 76th SEG annual international meeting, Denver, Expanded Abstracts, 4258–4262.

Landrø M. 2008. The effect of noise generated by previous shots on seismic reflection data. *Geophysics* 73, Q9–Q17.

Laws R.M. 2012a. *Simultaneous marine vibrators*. United States Patent Application, Publication No. US 2014/0334257 A1.

Laws R.M. 2012b. *Marine vibrator sweeps with reduced smearing and/or increased distortion tolerance*, Publication No. US2013/0343153A1.

Laws R.M. 2013. *Determining a seismic vibrator signature*. United States Patent Application, Publication No. US20140283615A1.

Laws R.M. and Halliday D.F. 2013. *Seismic data apparition from phase shifted sources*. United States Patent Application, Publication No. US 2017/0269241 A1.

Laws R.M., Halliday D.F., Özbek A. and Hopperstad J.-F. 2016. Exploiting the control of phase in marine vibrators. *First Break* 34, 65–74.

Laws R. and Kragh E. 2002. Rough seas and time-lapse seismic. *Geophysical Prospecting* 50, 195–208.

Laws R.M., Kragh E. and Morgan G. 2008. Are seismic sources too loud? 70th EAGE meeting, Rome, Expanded Abstracts, B026.

Laws R.M. and Morice S.P. 1999. *A method of seismic surveying, a marine vibrator arrangement, and a method of calculating the depths of seismic sources*. European Patent Office EP1214610B8.

Laws R.M., Parkes G.E. and Hatton L. 1988. Energy interaction: the long-range interaction of seismic sources. *Geophysical Prospecting* 36, 333–348.

Moerig R., Barr F.R. and Nyland L. 2002. Simultaneous shooting using cascaded sweeps. 72nd SEG annual international meeting, Salt Lake City, Expanded Abstracts, 2002-0074.

Moore I., Dragoset B., Ommundsen T., Wilson D., Ward C. and Eke D. 2008. Simultaneous source separation using dithered sources. 78th SEG annual international meeting, Las Vegas, Expanded Abstracts, 2806–2810.

Mosher C., Li C., Morley L., Ji Y., Janiszewski F., Olson R. *et al*. 2014. Increasing the efficiency of seismic data acquisition via compressive sensing. *The Leading Edge* 33, 386–391.

NOAA 2016. *Technical guidance for assessing the effects of anthropogenic sound on marine mammal hearing*, Underwater Acoustic Thresholds for Onset of Permanent and Temporary Threshold Shifts, NOAA Technical memorandum NMFS-OPR-55.

Özbek A., Vassallo M., Özdemir K., van Manen D.-J. and Eggenberger K. 2010. Crossline wavefield reconstruction from multicomponent streamer data: part 2 – joint interpolation and 3D up/down separation by generalized matching pursuit. *Geophysics* 75, WB69–WB85.

Popper A.N., Hawkins A.D., Fay R.R., Mann D.A., Bartol S., Carlson T.J. *et al*. 2014. *Sound exposure guidelines for fishes and sea turtles*. Technical report for ANSI- S3/SC1, ASA S3/SC1.4 TR-2014, ASA Press.

Potter G., Mann A., Jenkerson M. and Rodriguez J.M. 1997. Comparison of marine vibrator, dynamite, and airgun sources in the transition zone. 59th EAGE meeting, Geneva, Expanded Abstracts, B018.

Robertsson J.O.A., Amundsen L. and Pedersen A.S. 2016. Signal apparition for simultaneous source wavefield separation. *Geophysical Journal International* 206, 1301–1305.

Schonewille M., Dishberger D. and Kapadia D. 2014. Comparison of 3D time-domain radon and matching-pursuit Fourier interpolation. 84th SEG annual international meeting, Denver, Expanded Abstracts, 3605–3609.

Schonewille M., Klaedtke A. and Vigner A. 2009. Anti-alias anti-leakage Fourier transform. 79th SEG annual international meeting, Houston, Expanded Abstracts, 3249–3253.

Southall B.L., Bowles A.E., Ellison W.T., Finneran J.J., Gentry R.L., Greene C.R. *et al*. 2007. Marine mammal noise exposure criteria: initial scientific recommendations. *Aquatic Mammals* 33, 411–522.

Vassallo M., Özbek A., Özdemir K. and Eggenberger K. 2010. Crossline wavefield reconstruction from multicomponent streamer data: part 1 – multichannel interpolation by matching pursuit (MIMAP) using pressure and its crossline gradient. *Geophysics* 75, WB53–WB67.

Ziolkowski W.M., Parkes G.E., Hatton L. and Haugland K. 1982. The signature of an air gun array: computation from near-field measurements including interactions. *Geophysics* 47, 1413–1421.